Nucleic Acids Research, 2024, **52**, 223–242
https://doi.org/10.1093/nar/gkad1037
Advance access publication date: 13 November 2023
Genome integrity, repair and replication

The function of BCL11B in base excision repair contributes to its dual role as an oncogene and a haplo-insufficient tumor suppressor gene

Elise Vickridge[1], Camila C.F. Faraco[1,2], Fanny Lo[1,2], Hedyeh Rahimian[1], Zi Yang Liu[1,2], Payman S. Tehrani[3], Billel Djerir[4], Zubaidah M. Ramdzan[1], Lam Leduy[1], Alexandre Maréchal[4], Anne-Claude Gingras[3,5] and Alain Nepveu[1,2,6,7,*]

[1]Goodman Cancer Institute, McGill University, 1160 Pine Avenue West, Montreal, Quebec H3A 1A3, Canada
[2]Department of Biochemistry, McGill University, 1160 Pine Avenue West, Montreal, Quebec H3A 1A3, Canada
[3]Lunenfeld-Tanenbaum Research Institute, Sinai Health System, Toronto, Ontario Canada
[4]Department of Biology and Cancer Research Institute, Université de Sherbrooke, Sherbrooke, Quebec, Canada
[5]Department of Molecular Genetics, University of Toronto, Toronto, Ontario, Canada
[6]Department of Medicine, McGill University, 1160 Pine Avenue West, Montreal, Quebec H3A 1A3, Canada
[7]Department of Oncology, McGill University, 1160 Pine Avenue West, Montreal, Quebec H3A 1A3, Canada
[*]To whom correspondence should be addressed. Tel: +1 514 398 5839; Fax: +1 514 398 6769; Email: alain.nepveu@mcgill.ca

Abstract

Genetic studies in mice and human cancers established *BCL11B* as a haploinsufficient tumor suppressor gene. Paradoxically, *BCL11B* is overexpressed in some human cancers where its knockdown is synthetic lethal. We identified the BCL11B protein in a proximity-dependent biotinylation screen performed with the DNA glycosylase NTHL1. *In vitro* DNA repair assays demonstrated that both BCL11B and a small recombinant BCL11B$^{213\text{-}560}$ protein lacking transcription regulation potential can stimulate the enzymatic activities of two base excision repair (BER) enzymes: NTHL1 and Pol β. In cells, BCL11B is rapidly recruited to sites of DNA damage caused by laser microirradiation. *BCL11B* knockdown delays, whereas ectopic expression of BCL11B$^{213\text{-}560}$ accelerates, the repair of oxidative DNA damage. Inactivation of one *BCL11B* allele in TK6 lymphoblastoid cells causes an increase in spontaneous and radiation-induced mutation rates. In turn, ectopic expression of BCL11B$^{213\text{-}560}$ cooperates with the RAS oncogene in cell transformation by reducing DNA damage and cellular senescence. These findings indicate that BCL11B functions as a BER accessory factor, safeguarding normal cells from acquiring mutations. Paradoxically, it also enables the survival of cancer cells that would otherwise undergo senescence or apoptosis due to oxidative DNA damage resulting from the elevated production of reactive oxygen species.

Graphical abstract

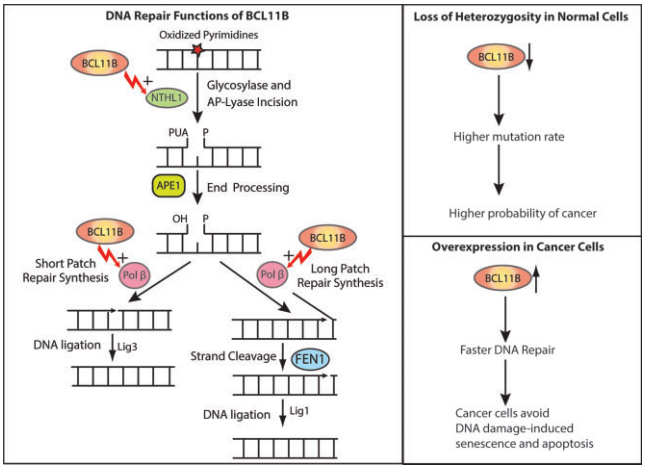

Received: June 14, 2023. **Revised:** October 13, 2023. **Editorial Decision:** October 17, 2023. **Accepted:** October 23, 2023

Introduction

Base excision repair (BER) repairs most base lesions including alkylated, deaminated and oxidized bases, as well as apurinic/apyrimidinic (AP) sites. This pathway is initiated by one of many DNA glycosylases which recognize specific base lesions and cleaves the N-glycosylic bond linking the altered base to the DNA backbone to produce an apyrimidinic/apurinic (AP) site (1,2). In mammals, AP sites are targeted by the AP endonuclease 1, APE1, which incises the DNA backbone 5′ to the AP site to generate a single-strand break with a 5′-deoxyribose phosphate (dRP) (3). In addition, DNA glycosylases for oxidized bases are also endowed with an AP/lyase activity that generates a single-strand nick 3′ to the AP site via beta (OGG1, NTHL1) or beta-delta (NEIL1, NEIL2) elimination (reviewed in (4)). 5′ or 3′ end processing of the resulting single-strand breaks are then performed by DNA pol β, APE1 or PNKP, and repair synthesis and ligation are accomplished by the short-patch or long-patch pathways (5–7). In short-patch repair, DNA pol β (Pol β) adds a single base and removes the 5′- dRP to allow ligation (8). In long patch repair, 2–13 bp are synthesized by Pol β or δ/ε, thereby generating a displaced strand that is cleaved by FEN1 prior to ligation (2,9). There is considerable overlap in substrate specificities among DNA glycosylases that repair oxidative DNA lesions, suggesting that redundancy has been built into the system (reviewed in (4)). However, in general, OGG1 is the primary repair enzyme for oxidized purines, whereas oxidative pyrimidine lesions are removed primarily by NTHL1, NEIL1 or NEIL2 (4).

Multiple connections have been reported between the BER pathway and transcription factors. On the one hand, several studies documented the role of the OGG1 DNA glycosylase in recruitment of transcription factors such as NFκB and the estrogen receptor (reviewed in (10)). On the other hand, several transcription factors and DNA binding proteins were shown to stimulate the enzymatic activity of one or several BER enzymes. YB-1 and hnRNP-U stimulate NEIL1 (11,12) HMGB1 stimulates the functions of the APE1 and FEN1 endonucleases (13). The FACT complex facilitates uracil removal by UDG (14). *In vitro,* P53 stimulates the activity of Pol β (15). CUT domains within CUX1, CUX2 and SATB1 stimulate OGG1 (16–19). CUT domains also stimulate the enzymatic activities of APE1 and Pol β to ensure repair completion (20,21).

The present study was initiated after we found that CUT domains do not stimulate glycosylases other than OGG1. We therefore hypothesized that other transcription factors may cooperate with distinct DNA glycosylases. As OGG1 exhibits specificity towards oxidized purines, we set out to identify accessory factors for the DNA glycosylase NTHL1 which is specific for oxidized pyrimidines. A proximity-dependent biotinylation screen with a NTHL1-BirA* protein uncovered the BCL11A and BCL11B proteins, which had previously been identified as oncogenes (22). We have shown that BCL11A stimulates the enzymatic activities of NTHL1 and Pol β and that its DNA repair function is required for triple-negative breast cancer cells to avoid senescence and continue to proliferate despite producing excess levels of reactive oxygen species (22). The implications of BCL11B in cancer are more complex since it has been characterized both as an oncogene and a haplo-insufficient tumor suppressor gene. *BCL11B* was identified as radiation-induced tumor suppressor gene 1 (Rit1) by studying γ-ray-induced mouse thymic lymphomas for losses of specific chromosomal DNA (23–26). Subsequent analysis in human T-cell acute lymphoblastic leukemias (T-ALL) revealed monoallelic *BCL11B* inactivating point mutations or deletions in 9–16% of cases (27–29). Heterozygous *Bcl11B* mice suffer higher incidence of thymic lymphomas after γ-radiation or crossing with p53 heterozygous mice (30–32). These genetic data clearly establish *BCL11B* as a haploinsufficient tumor suppressor gene. Paradoxically, BCL11B overexpression is reported in acute T-cell lymphomas, cutaneous T-cell lymphomas (CTCL), squamous cell carcinomas, Ewing sarcomas and glioblastomas (33–37). Notably, *BCL11B* knockdown is lethal in human T-cell leukemia, while normal mature T cells remain unaffected (30,38,39). In Ewing sarcomas, BCL11B represents a specific immunohistochemistry marker together with GLG1 and CD19 (40,41). Interestingly, *BCL11B* overexpression increases resistance to radiomimetic drugs and etoposide, however, the mechanism of action remains to be defined (42,43).

Mechanistically, BCL11B was originally identified as chicken ovalbumin upstream promoter transcription factor interacting protein 2 (CTIP2) (44). *BCL11B* encodes a Kruppel-like C2H2-type zinc finger transcription factor that binds to DNA and can function as a transcriptional repressor or activator depending on posttranslational modifications and promoter context (35,45–50). BCL11B is normally expressed in a tissue and cell-type specific manner, particularly in stem/progenitor cells (reviewed in (32,51)). Knockout mouse models reveal that BCL11B plays important roles in the development of several tissues, including T cells, the central nervous system (CNS), skin, tooth and the mammary gland (32,45,51). In particular, BCL11B specifies T cell fate (52–55). In human, several distinct heterozygous *de novo* mutations resulting in lower BCL11B expression or in the production of a truncated BCL11B protein cause a neurodevelopmental disorder, termed BCL11B-Related Disorder, characterized by speech impairment, intellectual disability, craniofacial anomalies, dermal defects, and immunological abnormalities (56–58). A case of severe combined immunodeficiency (SCID) associated with craniofacial and dermal abnormalities in a newborn was found to result from a heterozygous *de novo* missense *BCL11B* mutation, p.N441K. The dominant negative effect of this mutation was explained by the observation that the mutant protein forms nonfunctional heterodimers with the wild type BCL11B protein (59). Structure/function analysis identified an atypical CCHC zinc finger motif in the N-terminal region as being responsible for protein dimerization (60).

In the present study, we investigated the DNA repair functions of BCL11B in the BER pathway. In cancer cell lines that overexpress BCL11B we verified the effect of BCL11B knockdown on DNA repair and genomic DNA damage. We analyzed the functions of BCL11B in BER using *in vitro* DNA repair assays and defined the smallest peptide still able to stimulate the enzymatic activities of the NTHL1 DNA glycosylase and Pol β polymerase. We verified that a small peptide, devoid of transcription regulation potential, can rescue repair phenotypes resulting from BCL11B knockdown and cooperate with a RAS oncogene in cell transformation. We generated two independent clones of TK6 lymphoblastoid cells, in which one *BCL11B* allele has been inactivated, and measured their spontaneous and radiation-induced mutation rates using the fluctuation assays. Altogether our results establish that the DNA

repair functions of BCL11B are important for its roles as an oncogene and a haploinsufficient tumor suppressor gene.

Materials and methods

Cell culture and virus production

HEK293FT and U2OS cells were cultured in Dulbecco's modified Eagle's medium (DMEM, Wisent), Jurkat was cultured in Roswell Park Memorial Institute medium (RPMI, Wisent) and SKES-1 was cultured in McCoy 5A medium (Wisent). All media were supplemented with 10% fetal bovine serum (FBS, Gibco) and 1% penicillin streptomycin (Invitrogen). All cells were maintained at 37°C, 5% CO_2 and atmospheric O_2. Lentiviruses were produced by co-transfecting HEK293FT cells with plasmids encoding BCL11B full length, BCL11B EGFP, short hairpin RNA against BCL11B (Mission shRNA pLKO.1 library, Sigma) or plenti6V5-BCL11B$^{213–560}$ with packaging plasmid psPAX2 and envelop plasmid pMD2G. The medium of the transfected cells was collected for 3 days, 48 h post-transfection.

Plasmid construction

Plasmids expressing his-tagged BCL11B fragments (BCL11B$^{1–213}$, BCL11B$^{213–420}$, BCL11B$^{411–550}$, BCL11B$^{711–894}$ and BCL11B$^{213–560}$) were prepared by inserting gBlocks gene fragments (Integrated DNA Technologies) into pET-30a vector using restriction enzymes. C-His-BCL11B plasmid was purchased from GeneCopoeia in vector system pReceiver-B31. 3xHA–BCL11B$^{213–560}$ was cloned by inserting the gBlock fragment into plenti6V5 backbone by gateway cloning.

Bacterial protein expression

All proteins were expressed in the BL21 strain of *Escherichia coli*. Bacteria were cultured until they reached an optical density of 0.3–0.4 at 600 nm. Isopropyl-β-D thiogalactopyranoside was added to 1 mM and bacteria were incubated at 12°C for 20 h. In the case of his-tagged fusion proteins, nickel beads were washed several times in 20 and 40 mM imidazole, and elution was performed in 250 mM imidazole. Following elution from the nickel beads several buffer exchanges were carried in 3-kDa molecular weight cut-off dialysis membrane (Amicon Ultra, Millipore) to bring down imidazole concentration to less than 0.1 μM. In the case of the BCL11B$^{213–560}$ protein, in addition to a C-terminal His-tag, we added an N-terminal Strep-tag to be able to perform affinity chromatography over Strep-Tactin®XT resin according to the manufacturer's instructions (Iba, Göttingen, Germany).

Immunoblotting

Nuclear extracts were prepared according to the procedure of Lee *et al.* (61), except that nuclei were obtained by submitting cells to 3 freeze/thaw cycles in buffer A (10 mM HEPES, pH 7.9, 10 mM KCl, 1.5 mM $MgCl_2$, 1 mM DTT). Nuclei were then resuspended in Buffer C (20 mM HEPES, pH 7.9, 25% glycerol 1.5 mM MgCl2, 420 mM $NaCl_2$, 0.2 mM EDTA) and incubated at 4°C for 30 min. After 15 min of centrifugation, the supernatant was collected. Buffers A and C were supplemented with protease inhibitor mix tablet purchased from Roche. Whole cell extracts extracts were prepared by applying buffer X (50 mM HEPES, pH 7.9, 0.4 M KCl, 4 mM NaF, 4 mM Na_3VO_4, 0.2 mM EGTA, 0.2 mM EDTA, 0.1% NP-40, 10% glycerol, 0.5 mM DTT, protease inhibitor mix tablet from Roche) to a monolayer plate. After 10 min incubation on ice, the resulting slurry was centrifuged for 15 min at 4°C and the supernatant was collected.

For immunoblotting, protein extracts were recovered as described above and separated by electrophoresis on 6% polyacrylamide. For the primary antibody incubation, antibodies were incubated with the membrane in TBST (10 mM Tris pH8, 150 mM NaCl, 0.1% Tween) for 1 hour at room temperature. After four 10 min washes with TBST, secondary antibodies were added to membrane in TBST and incubated for 1h at room temperature. Following four 10 min washes with TBST, proteins were visualized with the ECL system from Amersham. The following antibodies and dilutions were used: anti-BCL11B (1:2000, Bethyl), anti-NTHL1 (1:1000, Proteintech), anti-GST (1:1000, Abcam), anti Pol β (1:1000, Abcam), anti-His (1:3000, Sigma), anti-HA (1:1000 Covance), anti-γ-tubulin (1:10 000, Sigma) and V5 antibody (1:1000 Sigma). Secondary HRP-conjugated antibodies, anti-mouse or anti-rabbit are from Jackson Laboratories (1:10 000).

Affinity purification

293T cells were co-transfected with 3xHA-BCL11B and c-avi NTHL1 (plasmids purchased by GeneCopoeia) using Lipofectamine3000 (Invitrogen) according to the manufacturer's instructions. 50 μM of biotin was added into the media 48 h after transfection, and cells were collected after 24 h. Cells were lysed in 20 mM Tris (pH 8.0), 150 mM NaCl, 1% NP40 supplemented with a protease inhibitor cocktail (Sigma) and centrifuged at 13 000 *g* for 20 min. c-avi NTHL1 was affinity-precipitated with magnetic streptavidin beads (GE Healthcare). The samples were separated by SDS-PAGE followed by immunoblotting with anti-NTHL1 antibody and anti-BCL11B antibody.

Split intein

293T cells were transfected with the following combinations of expression vectors: BCL11B -V5-IN and IC2-flag-NTHL1; IC2-flag-Pol β and BCL11B$^{213-560}$-V5-IN; BCL11B$^{213-560}$-V5-IN and IC2-flag-LIG3 or IC2-flag-FOXN2. No selection was performed. Total extracts were obtained with RIPA lysis buffer. For each sample, 40 μg were loaded onto an SDS PAGE gel and blotted against V5 (Cell Signaling Technologies) or Flag (Sigma).

GST-pull down assay

Bacterially expressed GST-tagged NTHL1 and bacteria carrying the empty GST tag vector were bound to glutathione-Sepharose beads (GE Healthcare) and incubated overnight at 4°C with 1 μg of purified his-tagged BCL11B fragments. The samples were washed three times NP40 lysis buffer (50 mM Tris pH 8), 150 mM NaCl, 1% NP40, 50 mM NaF and protease inhibitor) and separated by SDS-PAGE and proteins were visualized by immunoblotting against GST and His.

In vitro fluorescent cleavage assay

The fluorescent cleavage assay was performed as previously described (62), with minor modifications. We used a 43-mer oligonucleotide (Midland) with DHT modification at its sixth

position. The 5′ end of the DNA was conjugated to a FAM fluorophore, and 3′ end conjugated to a Dabcyl quencher. Cleavage reactions were conducted in a 25 μl reaction containing 50 nM of oligonucleotide, 10 nM of enzyme and proteins, in 20 mM Tris (pH 8), 1 mM EDTA (pH 8.0), 1 mM DTT. The reactions were incubated at 37°C, and fluorescence data were collected on a Realplex machine (Eppendorf Mastercycler) equipped with standard optics (excitation filter, 494 nm; emission filter, 520 nm). A linear regression model was used to determine the initial velocity of each enzymatic activity curve. The effects of each protein in the presence of 5 nM NTHL1 were determined from nonlinear regression of initial velocity versus concentration of proteins using Prism 6.0 (GraphPad).

In vitro radioactive cleavage assay

Double-stranded 32-mer oligonucleotides containing a Thymine-Glycol modification at the 18th position (Midland) were labeled with γ-P^{32}-dATP at the 5′ end of the top strand (*) using polynucleotide kinase. Cleavage reactions were conducted using indicated concentration of bacterially purified proteins and enzyme in 20 mM Tris (pH 8), 1 mM EDTA (pH 8.0), 1 mM DTT and 1 pmol of labeled probe. Reactions were performed for 30 min at 37°C and terminated by formamide DNA loading buffer (90% formamide with 0.05% bromophenol blue and 0.05% xylene cyanol). The DNA was loaded on a pre-warmed 20% polyacrylamide-urea gel (19:1) and separated by electrophoresis in Tris-borate and EDTA (TBE; pH 8.0) at 20 mA. The radiolabeled DNA fragments were visualized by storage phosphor screen (GE Healthcare).

Tg cleavage assay with a fluorophore-based probe

Double-stranded 32-mer oligonucleotides containing a thymine-glycol modification at the 18th position were labeled with 6-FAM fluorescein. Reactions were performed as described above for the radioactively-labeled probe, except that at the end of the reaction, samples were adjusted to 0.5% SDS and 20 mM EDTA, 1 mg/μl proteinase K and incubated for another 30 min.

Sodium borohydride trapping of NTHL1

5′-End-labeled 32-mer duplex containing a thymine–glycol modification was incubated with purified NTHL1, and BCL11B proteins or BSA at the indicated concentrations. After incubation at 37°C for 30 min, 50 mM sodium borohydride was added and the reactions were incubated for 15 min at 37°C. The trapped complexes were separated from free substrate by 10% SDS-PAGE gel.

Electrophoretic mobility shift assay (EMSA)

EMSAs with BCL11B proteins were performed using the indicated amounts of purified proteins and incubated at room temperature for 15 min in a final volume of 30 μl of 25 mM HEPES (pH 7.5), 50 mM KCl, 5 mM $MgCl_2$, 10 μM $ZnCl_2$, 5% glycerol, 0.1 M DTT, with 0.1 μg poly dIdC and 1 μg BSA as nonspecific competitors of DNA and protein. End-labeled double-stranded oligonucleotides (1 pmol) were added and further incubated for 15 min at room temperature. Samples were loaded on 5% native polyacrylamide gels and separated by electrophoresis at 100 V. Gels were dried and visualized by autoradiography. EMSAs with NTHL1 and Pol β were performed in a different buffer: 25 mM NaCl, 10 mM Tris, pH 7.5, 1 mM $MgCl_2$, 5 mM EDTA, pH 8.0, 5% glycerol, 1 mM of DTT, with 30 ng of poly dIdC and 30 μg of BSA as nonspecific competitors.

Laser microirradiation

U2OS stable cell populations expressing EGFP-BCL11B were seeded onto a 96-well plate with 170 μm glass bottom (Ibidi). Cells were imaged in real-time as described previously (63). Briefly, cells were pretreated with 2 μM Hoechst 33 342 (Sigma-Aldrich) for 5 min before being micro-irradiated using a FV-3000 Olympus confocal microscope equipped with a 405 nm laser line. The microscope was configured for the micro-irradiation step using the fluorescence-recovery after photobleaching (FRAP)_module of the system. A single line scan of the 405-nm laser at 70% power was sufficient to generate oxidized bases and activate the base excision repair pathway. Recruitment of GFP-BCL11B to micro-irradiation stripes was quantitatively monitored using the Damage Analyzer Fiji script (64). 12-bit images were collected at 1× zoom and processed using the Outliner Fiji script, The Outliner, which automatically outlines cell nuclei using a DNA dye-associated channel (e.g. DAPI). This script makes it easier to distinguish micro-irradiation stripes and individual cells by leaving out uninformative DNA staining from the final images. Output data were plotted using Microsoft Excel.

Single cell gel electrophoresis

Jurkat cells were plated at 300 000 cells/ml. SKES-1 and A673 cells were plated at 150 000 cells/ml. 50 μM of H_2O_2 was used to treat cells on ice for 20 min to induce DNA damage. Immediately after treatment, cells were washed with PBS to eliminate H_2O_2 residue and allowed to recover at 37°C in fresh medium for the indicated amount of time. For the comet assay performed at pH 10 with Endo III treatment, slides were immersed in lysis solution containing Endo III enzyme for 1h at 37°C prior to electrophoresis. For IMR90, the cells stably carrying $BCL11B^{213–560}$ were infected with pBABE—$HRAS^{G12D}$ or pBABE—empty vector. 48 h after infection, cells were selected with 4 μg/ml puromycin for 3 days and pelleted for comet assay. Comet assay was carried out as described in Ramdzan *et al.* (19).

Polymerase and strand-displacement activity with a fam-probe

The FAM- and DABCYL-linked oligodeoxynucleotides were purchased from Midland Oligos. The oligodeoxynucleotides were annealed and Pol β activity was performed as described (65). Briefly, the short complementary oligodeoxynucleotide primer (5′-TCACCCTCGTACGACTC) and reporter labeled with FAM (5′- TTTTTTTTTTTTTTTGC-FAM – 3′) were annealed, in 50 mM Tris–HCl, pH 8.0 and 100 mM NaCl, to an oligodeoxynucleotide template linked to DABCYL (5′- DABCYL – GCAAAAAAAAAAAAAAAGAGTCCATTAAGGGTGA-3′) to create double-stranded DNA substrates in which the FAM signal is quenched. The annealed oligonucleotides were then stored at –20°C as 50 μM stocks. The fluorophore-based probe (500 nM) was incubated with 5 nM of Pol β and 10 nM of BCL11B protein or BSA in the presence of 50 mM Tris–HCl, pH 8.0, 10 mM KCl, 1 mM $MgCl_2$, 2 mM DTT,

0.01% Tween-20, 500 ng BSA, 100 μM dTTP and 500 nM fluorescent probe.

Polymerase assays with radiolabeled probes

For the polymerase/elongation assay of Figure 5D, a 46-bp oligonucleotide containing uracil at position 20 (5′-TAGATGCCTGCAGCTGATGUGCCGTACGGATCC ACGTGTACGGTCA-3′) was labeled at its 5′end by T4 polynucleotide kinase and γ-^{32}P dATPs, annealed with the complementary oligonucleotide (5′-TGACCGTACACGTGG ATCCGTACGGCGCATCAGCTGCAGGCATCTA-3′) and purified on a 12% non-denaturing gel. Prior to each assay, the ^{32}P-labeled uracil containing duplex oligodeoxynucleotide was pre-treated for 15 min at 37°C with uracil–DNA glycosylase and APE1 to create an abasic site and produce a nicked substrate for Pol β. The polymerase reactions were performed in 50 mM Tris–HCl, pH 8.0, 10 mM KCl, 1 mM $MgCl_2$, 2 mM dithiothreitol, 0.01% Tween-20 with 20 nM Pol β and 10 nM of either HOXB3 or BCL11B$^{213–560}$ or 360 nM BSA in the presence of cold dNTPs.

Polymerase β deoxyribose phosphate (dRP)-lyase activity

A 32-bp oligonucleotide containing uracil at position 18 (5′-CCGGTGCATGACACTGTUACCTATCCTCAGCG-3′) was labeled at its 3′end with the Klenow fragment and CF 660R dCTP. The radiolabeled oligos were purified on a 12% non-denaturing gel and resuspended in Tris-EDTA buffer. Just prior to each dRP lyase assay, the fluorescent labeled uracil containing duplex oligodeoxynucleotide was pre-treated for 15 min at 37°C with uracil–DNA glycosylase (UDG) and APE1. The dRP-lyase reactions were performed as previously described, with some modifications (66). Reactions took place in 50 mM Tris–HCl, pH 8.0, 10 mM KCl, 1 mM $MgCl_2$, 2 mM dithiothreitol, containing 0.01% Tween-20 with 200 nM fluorescent labeled DNA and 10 nM of purified Pol β (ENZ-168; ProspecBio). The reactions were terminated with EDTA, and the product was stabilized by addition of sodium borohydride ($NaBH_4$) to a final concentration of 340 mM and incubated for 30 min at 4°C. The stabilized DNA product was recovered by ethanol precipitation in the presence of 20 μg of glycogen and 200 mM NaOAC. The precipitated DNA was then resuspended in 20 μl of gel loading buffer. After incubation at 75°C for 2 min, the DNA was loaded on a pre-warmed 20% polyacrylamide-urea gel (19:1) and separated by electrophoresis in Tris-Taurine and EDTA (TTE; pH 8.0) at constant 50V.

Senescence quantification

IMR90 cells stably expressing BCL11B$^{213-560}$ or carrying the empty vector were infected with pBABE -HRAS^{G12V} or pBABE -empty vector. 48h after infection, cells were selected with 4 μg/ml puromycin. On day 5, cells were counted and plated to perform the β-galactosidase senescence assay the next day, on day 6. β-gal senescence was measured by flow cytometry (BD LSR Fortessa) following the instructions of the Spider-βgal senescence kit from Dojindo.

CFSE proliferation assay

SKES-1 cells were infected with a lentivirus expressing a BCL11B shRNA. On day 6, cell proliferation was measured by staining with CellTrace™ CFSE according to manufacturer's instructions. CFSE was added to the medium and a portion of the population was fixed immediately as the '0' generation. The remaining cells were allowed to proliferate for 4 days. Cells were fixed and analyzed by flow cytometry. The peaks within the CFSE profiles represent successive generations, as indicated above the peaks. The proliferation index is the total number of divisions divided by the number of cells that went into division.

Apoptosis assay

SKES-1 cells overexpressing BCL11B$^{213-560}$ were infected with a lentivirus expressing shBCL11B or an empty vector. 3 days after puromycin selection (0.2 ug/ml), cells were treated for apoptosis assay following the manufacturer's instructions (BD biosciences cat. no. 556 547). Briefly, 1 million cells were re-suspended in 1 ml of 1× binding buffer. 100 000 cells were transferred to a new tube and 5 μl of annexin V and 5 μl of propidium iodide were added to cells and incubated for 20 min at RT in the dark. After incubation, 400 μl of 1× binding buffer were added and cells were immediately analyzed by flow cytometry.

On/Off rate of DNA binding

EMSAs were performed using indicated amount of purified proteins and incubated at room temperature for 15 min in a final volume of 30 μL of 25 mM HEPES (pH 7.5), 50 mM KCl, 5 mM $MgCl_2$, 10 μM $ZnCl_2$, 5% glycerol, 0.1 M DTT, with 0.1 μg poly dIdC and 1 μg BSA as nonspecific competitors of DNA and protein.

On rate: End-labeled double-stranded oligonucleotides (0.1 pmol) were added to incubate for the indicated amount of time.

Off rate: End-labeled double-stranded oligonucleotides (0.1 pmol) were added to incubate for 15 min to establish stable binding. 100 pmol of unlabeled oligonucleotides of the identical sequence were added for the indicated amount of time.

Samples were loaded on 5% native polyacrylamide gels and separated by electrophoresis at 100V. Gels were dried and visualized by autoradiography.

Abasic site quantification

SKES-1 cells expressing BCL11B$^{213–560}$ or an empty vector were infected with a lentivirus carrying an shRNA against BCL11B or an empty vector. Jurkat cells expressing BCL11B$^{213–560}$ and/or an shRNA against BCL11B under the control of a doxycycline-inducible promoter were treated with doxycycline. Three days after infection or doxycycline induction, 5 million cells were pelleted. DNA extraction was performed with a DNA extraction kit (Qiagen) and aldehyde-reactive probe labeling and quantification of abasic sites were performed as described by an AP-sites assay kit (Dojindo Molecular Technologies).

Clonogenic viability assay

Clonogenic ability of irradiated cells was conducted as described previously (67). Briefly, 100–250 cells were then plated in either 60 mm or 6-well plates in triplicate. Different cell densities were plated to ensure that sufficient cell colonies were observed in all conditions. After 10–14 days of incubation, cells were washed with phosphate-buffered saline

(PBS), fixed with cold methanol for 20 min then stained with 0.1% crystal violet (Acros Organics) in 20% methanol for 30 min. The number of colonies with 50 cells or more was counted. Clonogenic efficiency is represented as the percentage of seeded cells that gave rise to clones under control conditions (no treatment). The reported values are the averages ± standard deviations.

Soft agar colony formation assay

IMR90 cells stably expressing BCL11B$^{213–560}$ or carrying the empty vector were infected with pBABE -HRAS^{G12D}. 48 h after infection, cells were counted and plated for soft agar colony formation assay. Briefly, cells were counted and resuspended to 40 000 cells/ml. A first layer of 1 ml of 0.6% medium-agarose was added to the 6-well plates (for each condition, triplicate wells were plated). Cells at 40 000 cells/ml were then mixed with 0.6% agarose at a ratio of 1:1. Then, 1 ml of agarose-mixed cells was added to the 0.6% agarose layer. Plates were left to solidify for 30 min and 500 µl of fresh DMEM was then added to the top layer. An extra 500 µl of DMEM was added after 4 days at 37°C. After 10 days, 500 µl of thiazolyl blue (at 1 mg/ml) were added to each well and plates were left at 37°C overnight. Colonies were counted the next day.

Oligonucleotide sequences

Fluorescent cleavage:

(X = dihydrothymine)

5′(FAM) CCACTXTTGAATTGACACGCCATGTCGA TCAATTCAACAGTGG (3′-Dabcyl)3′

Radioactive cleavage/Schiff base trapping assay:

(X = thymine glycol, sequences modified from (68))

5′ CCGGTGCATGACACTGTXACCTATCCTCAGCG 3′

3′ GGCCACGTACTGTGACAATGGATAGGAGTCGC 5′

EMSA/On/off rate/ KD calculation:

5′CCGGTAACCACATGATGCTTGCCTAGTGCTATC CTCA 3′

3′GGCCATTGGTGTACTACGAACGGATCACGATAG GAGTCGC 5′

Generation of BCL11B$^{+/-}$ heterozygous TK6 cells using CRISPR/Cas

To increase the probability of obtaining heterozygous clones, TK6 cells were electroporated with the CRISPR/Cas protein (Alt-R® S.p. Cas9 Nuclease V3, 100 µg, IDT catalog number 1 081 058) together with one of three single-guide RNAs.

#1, CAGGUGGUCAUCUUCGUCGG, nt 857–876 of BCL11B cDNA;

#2, GAUCCCGAUCUCCACCGGCU, nt 827–846;

#3, ACUUGGAUCCCGAUCUCCAC, nt 832–851

Fluctuation assay to measure mutation rates in the *HPRT* gene

To calculate spontaneous mutation rates, after counter-selection to eliminate pre-existing HPRT-minus cells, 5 cells/well were plated in 2 × 96 well plates to calculate the plating efficiency (69). In parallel, 24 wells were seeded with 100 cells per well. These 24 independent cultures were allowed to expand up to 8 million. At that point, 40 000 cells/well were plated in 2 × 96 well plates supplemented with 6-thioguanin. Twelve days later, the presence of positive wells was investigated in each of the 24 cultures.

To calculate radiation-induced mutation rates, following counter-selection to eliminate pre-existing HPRT-minus cells, 1 million cells were irradiated at 1.5 Gy. Then 5 cells/well were plated in 2 × 96 well plates to calculate the plating efficiency (69). In parallel, 24 wells were seeded with 800 cells per well. These 24 independent cultures were allowed to expand up to 8 million cells before being plated at 40 000 cells/well in 2 × 96 well plates supplemented with 6-thioguanin.

The mutation rate was calculated using the following equation where P_0 is the number of populations without mutants, P is the total number of populations (26), N_0 is the total number of cells plated for the mutation rate (7 680 000), and CE is the clonogenic efficiency (70).

$$MR = -\frac{\ln(P_0/P)}{CE \times N_0}$$

Results

Interaction between NTHL1 and BCL11B

The BCL11B protein was identified in a proximity-dependent biotinylation (BioID) assay performed with a fusion protein containing NTHL1 fused to the R118G mutant *E. coli* biotin conjugating enzyme BirA, commonly designated BirA* (22). A complete list of retained preys can be found in supplementary table 1 of that article (22). The interaction between NTHL1 and BCL11B in cells was confirmed by two approaches. First, we performed a pull-down using streptavidin beads and protein extracts from cells expressing BCL11B and NTHL1 fused to an AviTag. The BCL11B protein is clearly visible in the affinity precipitate (Figure 1A, lane 4). As a second approach, we took advantage of the recently developed method of Split Intein-Mediated Protein Ligation, whereby fusion proteins that respectively carry the N- and C-terminal portion of a modified Intein protein can recombine to produce a third fusion protein (71). A diagram illustrating this method is presented in Supplementary Figure 3A. Co-expression of BCL11B-V5-IN4b with IC2-FLAG-NTHL1 led to the production of a third fusion protein, BCL11B-V5-FLAG-NTHL1 that can be detected with both the FLAG and V5 antibodies (Figure 1B, lane 3).

BCL11B knockdown causes an increase in genomic DNA damage and a delay in the repair of oxidized bases and abasic sites

We verified the effect of BCL11B knockdown on genomic DNA damage and DNA repair in cell lines derived from cancers in which BCL11B is overexpressed. In SKES-1 sarcoma cells, BCL11B knockdown with two distinct shRNAs caused a significant increase in genomic DNA damage, as judged from single-cell gel electrophoresis (Figure 2B, non-treated). Similar results were obtained in Jurkat T-lymphoma cells and A673 sarcoma cells (Supplementary Figure 1A and 1C, non-treated). To assess the effect of BCL11B knockdown on DNA repair, we submitted cells to H_2O_2 exposure and allowed them to recover for different periods of time before performing comet assays. BCL11B knockdown in SKES-1 cells caused a significant delay in DNA repair (Figure 2B). Similar DNA repair delays were observed in Jurkat T-lymphoma cells and A673 sarcoma cells (Supplementary Figure 1A and 1C). We also performed comet assays at pH 10 following treatment of cells with the

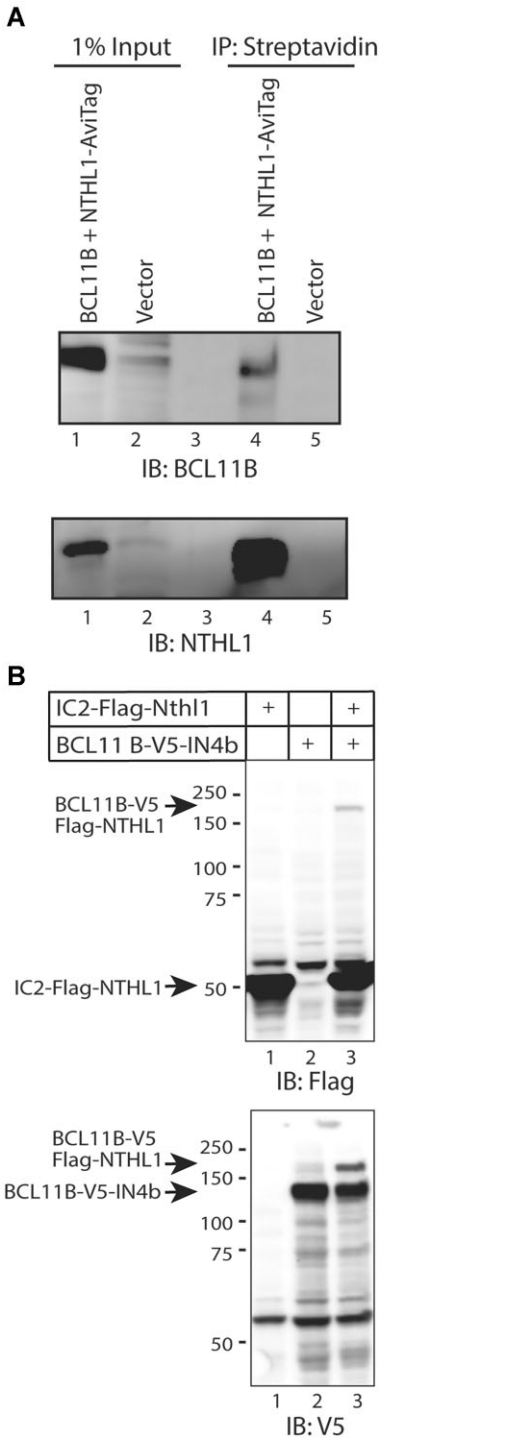

Figure 1. BCL11B interacts with the NTHL1 glycosylase. (**A**) HEK293FT cells were transfected or not with two vectors respectively expressing BCL11B and NTHL1-AviTag. 20 μM of biotin was added into the media 48 hr after transfection, and cells were collected after 24 hr. Affinity precipitation was performed using magnetic streptavidin beads, followed by immunoblotting with BCL11B and NTHL1 antibodies. Input (1%) was loaded as a protein expression control. (**B**) 293 cells were transfected with vectors expressing fusion proteins containing either the N-terminal or C-terminal portion of Intein, as indicated: IC2-Flag-NTHL1 and BCL11B-V5-IN4b. Whole cell extracts were submitted to immunoblotting analysis with the V5 and FLAG antibodies.

E. coli Endo III DNA glycosylase. Comet assay performed at pH 10 only detects DSBs and SSBs; however, pre-treatment with a DNA glycosylase allows the detection of a specific type of altered base. In particular, the *E. coli* NTH DNA glycosylase allows the detection of a variety of oxidized pyrimidines such as thymine glycol, 5-hydroxycytosine, 5-hydroxyuracil, as well as Fapy-purine residues (72). BCL11B knockdown was seen to cause a delay in the repair of oxidized bases (Figure 2E, pH 10 + EndoIII). Moreover, we also observed a drastic increase in the number of abasic sites in the genome of SKES-1 cells (Figure 2F). Increases in abasic sites following BCL11B knockdown were also observed in Jurkat and A673 cells (Supplementary Figure 1B and 1C). In summary, BCL11B knockdown causes a delay in DNA repair and an increase in genomic DNA damage in cancer cells where it is overexpressed.

BCL11B Is recruited to sites of DNA damage induced by laser-microirradiation.

To investigate whether BCL11B plays a direct role in the response to DNA damage, we expressed a fusion protein containing the green fluorescent protein fused to the N-terminus of BCL11B and submitted cells to laser-microirradiation. Of relevance to the present study, recruitment of NTHL1 and other BER enzymes to DNA lesions has previously been documented following laser micro-irradiation with similar conditions (73,74). We observed co-localization of γ-H2AX and GFP-BCL11B 2 minutes after irradiation (Figure 3A). Using timelapse imaging, we observed recruitment of GFP-BCL11B on the DNA damage track at 1min post-irradiation (Figure 3B). The signal remained strong at 2 min, decreased at 3 and 4 min and disappeared after 5 min (Figure 3B). Analysis of BCL11B-GFP recruitment in 12 independently microirradiated cells revealed an enrichment peak at 100 s, followed by a strong decline during the next 300 s, then a slower decline during the next 600 s.

BCL11B stimulates the enzymatic activities of NTHL1 *In Vitro*

We next verified the effect of BCL11B on the enzymatic activities of NTHL1. Proteins were purified from bacteria and incubated in the presence of a FAM-fluorophore probe containing a 5,6-dihydrothymidine (DHT) base at position 6 and a dabcyl quencher that resides next to the fluorophore upon annealing of the probe (Figure 4A). As shown in the diagram, removal of the DHT base followed by the introduction of a single-strand break through the AP/lyase activity of NTHL1 will release a short single-strand fragment with the fluorophore, away from the quencher (Figure 4A). The BCL11B protein stimulated the enzymatic activities of NTHL1 (Figure 4A). As controls, NTHL1 was incubated in the presence of BSA, HOXB3 or a CUX1 protein containing the CUT domains 1 and 2, which was previously shown to stimulate OGG1 enzymatic activities (17,19). As a second assay, we used a radiolabeled double-stranded oligonucleotide that contains a thymine-glycol (Tg) base (Figure 4B). Addition of BCL11B to the reaction increased the production of a cleaved fragment by NTHL1 (Figure 4B, compare lane 6 with lanes 7–10). As a further confirmation of these results, incubation in the presence of sodium borohydride showed that BCL11B stimulates the formation of a Schiff base between NTHL1 and the radioactively labeled probe (Figure 4C, compare lanes 5 and 6).

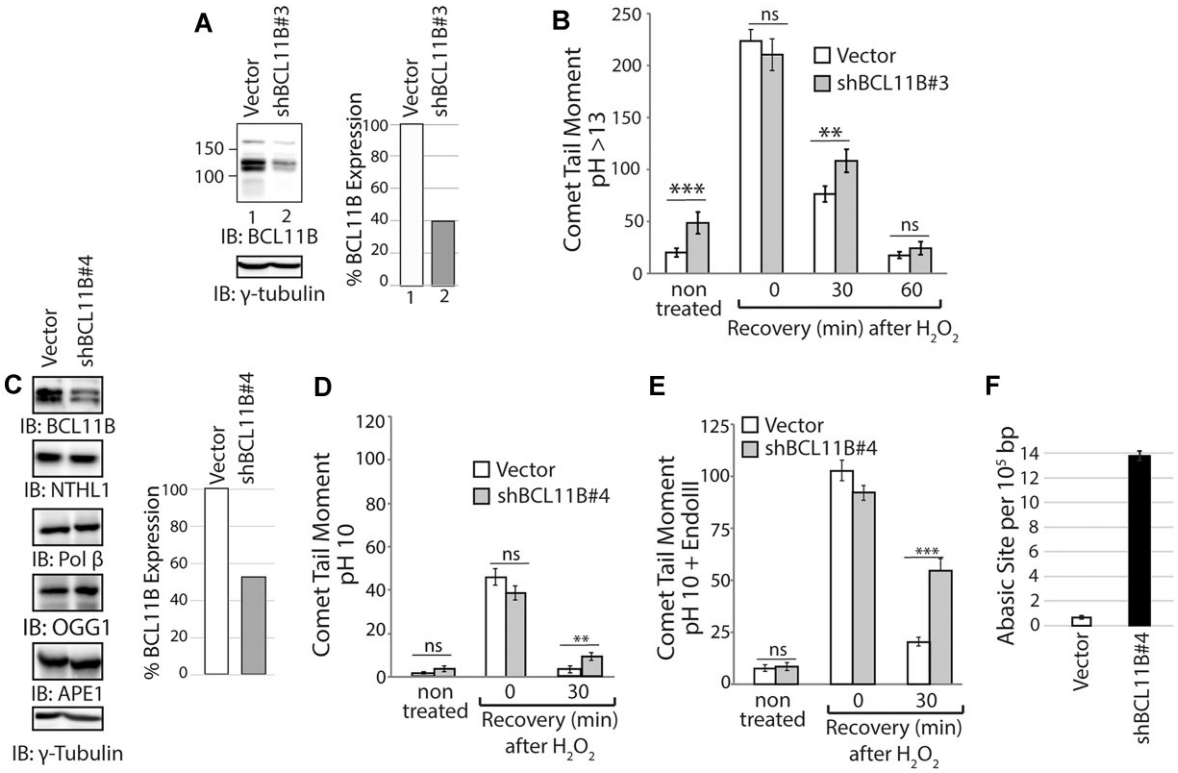

Figure 2. Knockdown of BCL11B leads to an increase of DNA damage (A, B) SKES-1 sarcoma cells were infected with lentiviral vectors expressing the BCL11B shRNA #3 or nothing. (**A**) Immunoblotting analysis.(**B**) Cells were exposed or not to 50 μM H_2O_2 for 20 min and allowed to recover for the indicated time before carrying out single cell gel electrophoresis at pH > 13. Comet tail moments were scored for at least 100 cells per condition. Results are a representative of one of three different experiments. Error bars represent standard error. ***$P < 0.001$; **$P < 0.01$; *$P < 0.05$; Student's *t*-test. (C–F) SKES-1sarcoma cells were infected with lentiviral vectors expressing the BCL11B shRNA #4 or nothing. (**C**) Immunoblotting analysis. (D, E) Cells were exposed or not to 50 μM H_2O_2 for 20 min and allowed to recover for the indicated time before carrying out single cell gel electrophoresis at pH 10 (**D**), and pH10 after treatment with the Endo III DNA glycosylase (**E**). Comet tail moments were scored for at least 100 cells per condition. Results are a representative of one of three different experiments. Error bars represent standard error. ***$P < 0.001$; **$P < 0.01$; *$P < 0.05$; Student's *t*-test. (**F**) Genomic DNA was purified and abasic sites were quantified using an aldehyde-reactive probe.

Structure-function analysis of BCL11B defines a region that interacts with NTHL1 and stimulates its enzymatic activity

We next expressed and purified recombinant proteins containing various regions of the BCL11B protein (Figure 4D and Supplementary Figure 2A and B). In pull-down assays using His-tagged BCL11B proteins with GST or GST-NTHL1, we observed an interaction between GST-NTHL1 and the $BCL11B^{213–420}$ and $BCL11B^{411–550}$ proteins, although the latter protein was also pulled down by GST alone, albeit to a lesser extent (Figure 4E, lanes 3–6). Neither of these proteins significantly stimulated NTHL1 enzymatic activities in the DHT cleavage assay with the FAM-fluorophore probe, however, a protein containing the amino acids present in both, $BCL11B^{213–560}$, was able to stimulate NTHL1 (Figure 4F). Stimulation of NTHL1 by $BCL11B^{213–560}$ was confirmed using the radiolabeled probe containing a thymine glycol base (Figure 4G, compare lanes 3 and 5). As the Tg-cleavage assays in Figure 4B and G were performed with different batches of purified NTHL1, we repeated these assays with a third batch of NTHL1 this time using 6-FAM fluorescein labeled double-stranded oligonucleotides (Figure 4H). The assays were performed three times to compare Tg-cleavage by NTHL1 in the presence of either BSA, BCL11B or $BCL11B^{213-560}$. Quantification of the substrate and cleaved product bands indicate that both BCL11B and $BCL11B^{213-560}$ stimulated cleavage approximately 2-fold (Figure 4H).

Importantly, the two probes that were used in the *in vitro* DNA repair assays did not contain a consensus BCL11B binding site. Moreover, the $BCL11B^{213–560}$ protein does not include the C-terminal zinc fingers that are responsible for DNA binding. Indeed, in addition to the full-length protein, only the $BCL11B^{711–894}$ protein is able to bind with high affinity to DNA that contains a BCL11B binding site (Supplementary Figure 2C, lanes 2, 9 and 10). Of note, both the full-length BCL11B protein and the $BCL11B^{711–894}$ fragment exhibit very fast DNA binding kinetics: they bind to DNA in less than one minute (Supplementary Figure 2D and 2E, on rate, lanes 9), and they are released from DNA in <1 min (Supplementary Figure 2D, compare lanes 4 and 11; Supplementary Figure 2E, compare lanes 11 and 12). This finding suggests that BCL11B may not remain bound to its preferred binding site for extended periods of time.

BCL11B interacts with pol β

The increase in the number of genomic abasic sites following BCL11B knockdown (Figure 2F and Supplementary Figure 1B and C) suggested that BCL11B may act on a downstream BER step. This observation was reminiscent of previous results with CUX1 that stimulates the enzymatic activities of OGG1 and Pol β and with BCL11A that stimulates the enzymatic activities of NTHL1 and Pol β (17,20,22). As an approach to verify the interaction between BCL11B and Pol β, we performed the

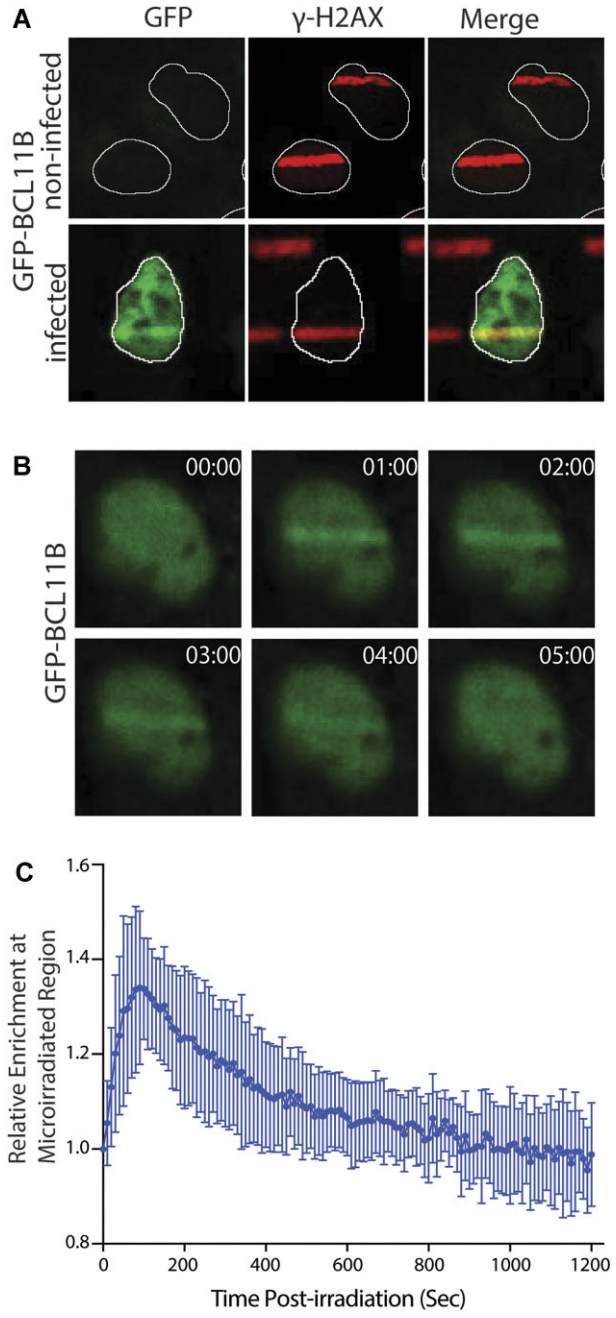

Figure 3. BCL11B is recruited to sites of DNA damage induced by laser micro-irradiation. (**A**) U2OS cells were infected or not with a lentivirus expressing BCL11B fused to a GFP protein and DNA damage was induced by laser micro-irradiation at 405 nm. Cells were fixed and stained for γ-H2AX by immunofluorescence at 2 min post-irradiation. The GFP signal was obtained, and the two images were merged. (**B**) Timelapse imaging of BCL11B-GFP recruitment to the sites of DNA damage after laser micro-irradiation. The 00:00 time point was taken before micro-irradiation. (**C**) Recruitment of BCL11B-GFP to micro-irradiation stripes was quantitatively monitored using the Damage Analyzer Fiji script (106). Output data were plotted using Prism. The blue points are the mean enrichment-fold of BCL11B-GFP at micro-irradiated sites relative to the pre-irradiation signal and the error bars represent the standard error of the mean of 12 independently micro-irradiated cells.

split intein assay (71). Co-expression of BCL11B$^{213–560}$-V5-IN with IC2-FLAG-Pol β led to the production of a new fusion protein, BCL11B$^{213–560}$-V5-FLAG-Pol β, that is detected with both the V5 and FLAG antibodies (Figure 5A, lane 3). In contrast, co-expression of BCL11B$^{213-560}$-V5-IN with either C2-FLAG-LIG3 or C2-FLAG-FOXN2 did not generate a new fusion protein (Supplementary Figure 3B, lanes 2 and 4). In pull-down assays, we observed an interaction between GST-Pol β and the His-tagged BCL11B$^{213-420}$ protein (Figure 5B, lane 4).

BCL11B stimulates pol β enzymatic activities

We performed a series of *in vitro* DNA repair assays to monitor whether BCL11B can stimulate the enzymatic activities of Pol β. Using a FAM fluorophore-based probe containing a nick, we observed that BCL11B and BCL11B$^{213–560}$ stimulate strand-displacement by Pol β (Figure 5C). Using 5′ end-labeled double-stranded oligonucleotides containing an abasic site, we observed that the BCL11B$^{213–560}$ peptide was able to stimulate the addition of several nucleotides by Pol β (Figure 5D, compare lane 2 with lanes 1 and 3). As controls, the reactions were performed in the presence of either BSA or HOXB3 (Figure 5D, lanes 1 and 3).

Another important enzymatic activity of Pol β involves the conversion of a 5′-deoxyribose phosphate (dRP) into a 5′-phosphate (P) to enable the final ligation step. The dRP-lyase activity of Pol β was previously shown to represent a rate-limiting step in base excision repair (75,76). We prepared a fluorescently labeled DNA probe containing a single-strand break with a 5′end dRP residue (Figure 5E, diagram). Note that the dRP residue is a labile chemical group, but its conversion into phosphate can be limited by adding $NaBH_4$ to the reaction (Figure 5E, compare lane 1 with lane 2 in which NaCl was replaced with $NaBH_4$). The probe was incubated with Pol β in the presence of either BSA or BCL11B$^{213–560}$. Importantly, in the absence of Pol β, we did not observe any conversion of dRP into P (Figure 5E, lanes 2 to 4). The dRP-lyase activity of Pol β was stimulated in the presence of BCL11B$^{213–560}$ at the 15 min time point (Figure 5E, compare lane 5 with 6).

BCL11B stimulates the binding of NTHL1 and pol β to their substrate

In previous work with another BER auxiliary factor, we observed that the CUT domains stimulate the binding of OGG1 and Pol β to their respective substrates (17) and unpublished observations). We therefore verified whether the same mechanism is at play in the case of BCL11B. In these electrophoretic mobility shift assays (EMSAs), we used conditions that did not enable enzymatic activities to be able to catch the enzyme as it binds to its substrate. EMSAs with a probe containing a thymine glycol base showed that the BCL11B$^{213–560}$ peptide was able to enhance the binding of NTHL1 to its substrate (Figure 6A, compare lanes 1 and 3, lanes 2 and 4, lanes 5 and 7, and lanes 6 and 8). Likewise, the BCL11B$^{213-560}$ peptide increased the binding of Pol β to double-stranded DNA that contains a single-strand break with a 5′-dRP group (Figure 6B, compare lane 1 with lanes 2, 3 and 4 and lane 11 with lanes 12, 13 and 14). However, the BCL11B$^{213–560}$ peptide on its own did not form a retarded complex with either probe (Figure 6A, lane 9; B, lane 9).

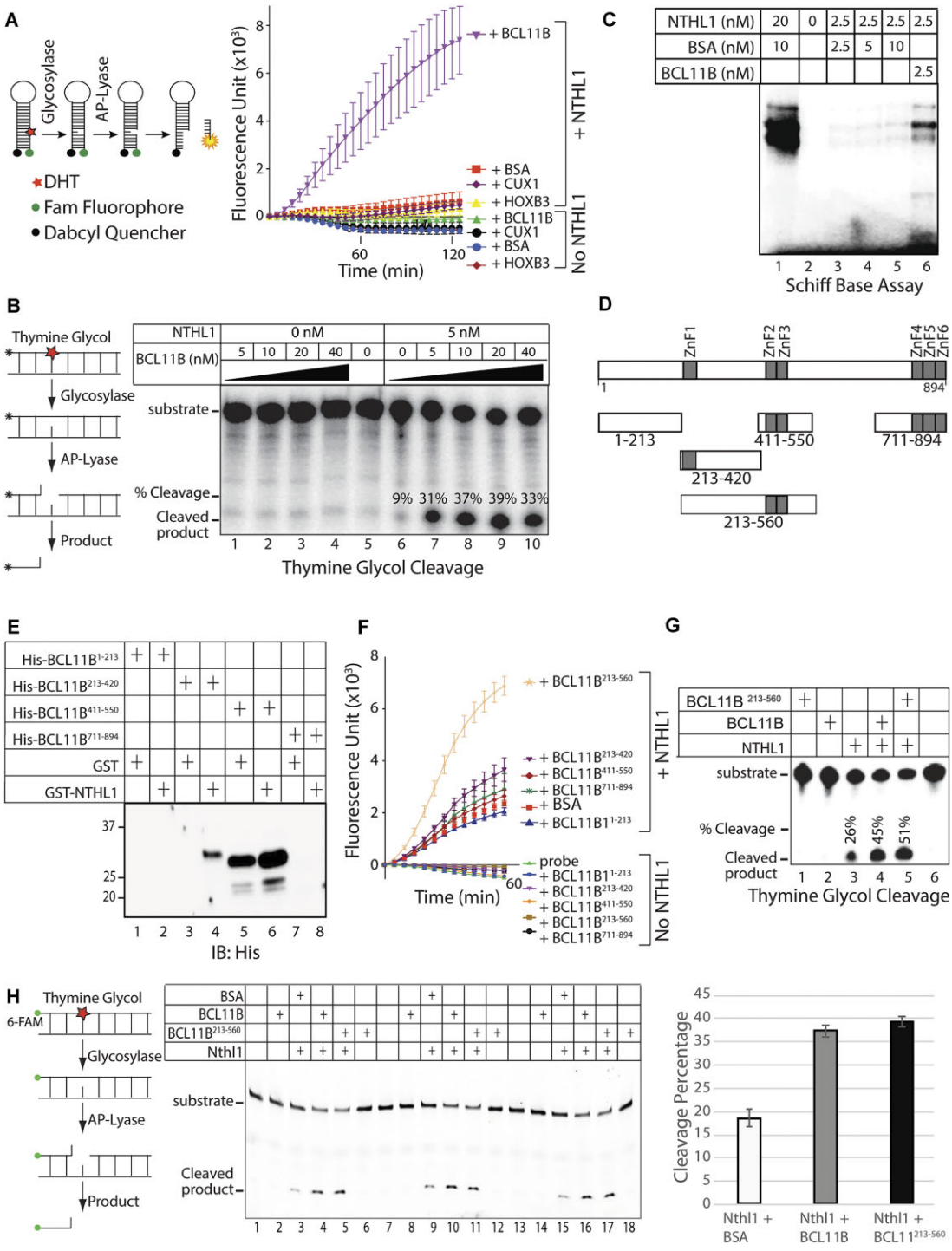

Figure 4. BCL11B and a small recombinant protein, BCL11B$^{213-560}$, stimulate NTHL1 enzymatic activity. (**A**) Diagrammatic representation of the 5,6-dihydrothymidine (DHT) cleavage assay using a fluorophore reporter probe. The assay was performed using 5 nM of NTHL1 and 20 nM of BCL11B full length protein or HOXB3, in the presence of 50 nM of BSA. (**B**) Diagrammatic representation of the thymine glycol (Tg) cleavage assay using a radioactively labeled probe. The assay was performed using purified NTHL1 (5 nM) and increasing amounts of BCL11B full length protein, as indicated. (**C**) Schiff base assay: radioactively end-labeled double-stranded oligonucleotides containing a thymine glycol (Tg) base were incubated with the indicated amount of NTHL1, BSA and BCL11B proteins. After incubation at 37°C, 50 mM sodium borohydride was added. The reactions were incubated for another 15 min at 37°C. After termination of the reaction, the trapped complexes were separated from free DNA by 10% SDS-PAGE. (**D**) Diagrammatic representation of the full-length BCL11B protein and smaller BCL11B proteins that were purified from bacteria and tested in DNA repair assays. (**E**) Pull-down assays were performed using His-tagged BCL11B fragments and either GST or GST-NTHL1, followed by immunoblotting with anti-His antibodies. (**F**) DHT cleavage assays were performed using 20 nM of BCL11B fragments, in the presence or absence of NTHL1 (5 nM), as indicated. All samples included 50 nM of BSA; the sample labeled 'BSA' included an additional 20 nM BSA. (**G**) Thymine-glycol (Tg) cleavage assays were performed using radioactively end-labeled double-stranded oligonucleotides containing a Tg oxidized base, and 250 nM BSA. Where indicated, NTHL1 (2.5 nM), BCL11B full length or BCL11B$^{213–560}$ (15 nM) were included in the reaction. (**H**) Thymine-glycol (Tg) cleavage assays were performed using 6-FAM fluorescein labeled double-stranded oligonucleotides containing a Tg oxidized base, and 250 nM BSA. Where indicated, NTHL1 (5 nM), BCL11B full length or BCL11B$^{213–560}$ (15 nM) were included in the reaction.

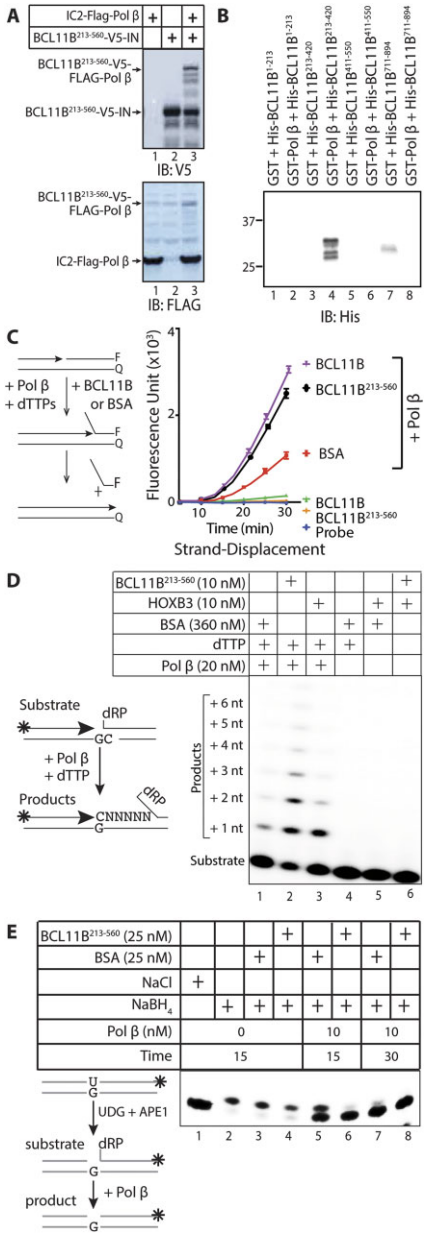

Figure 5. BCL11B$^{213–560}$ recombinant protein interacts with Pol β and stimulates its activity. (**A**) 293 cells were transfected with vectors expressing fusion proteins containing either the N-terminal or C-terminal portion of Intein, as indicated: BCL11B$^{213–560}$-V5-IN4b or IC2-Flag-Pol β. Whole cell extracts were submitted to immunoblotting analysis with the V5 and FLAG antibodies. (**B**) Pull-down assays were performed using His-tagged BCL11B fragments and either GST or GST-Pol β, followed by immunoblotting with anti-His antibodies. (**C**) Diagrammatic representation of the strand displacement assay using a fluorophore reporter probe. F: FAM fluorophore; Q: Quencher. The strand displacement assay was performed using 10 nM of BCL11B and 5 nM of Pol β. 50 nM of BSA were added to each reaction. (**D**) Double-stranded oligonucleotides containing a uracil residue were labeled at the 5′-end and incubated with UDG and APE1 to form a gapped substrate for Pol β. The gapped probe was then incubated with all 4 dNTPs in the presence of 20 nM of Pol β and either10 nM BCL11B$^{213-560}$ or 10 nM HOXB3 or 360 nM BSA as negative controls. (**E**) Double-stranded oligonucleotides containing a uracil residue, that were labeled at the 3′ end using Klenow and fluorescent CF 660R dCTP, were incubated with UDG and APE1 to produce a single-strand nick with a 5′-deoxyribose phosphate (dRP). This DNA substrate was incubated with Pol β in the presence of BSA or BCL11B$^{213–560}$. Except for the first lane, NaBH4 was added to all samples to prevent the spontaneous conversion of dRP into P.

Ectopic expression of the BCL11B$^{213–560}$ fragment accelerates DNA repair and increases resistance to oxidative DNA damage

As a first step to verify whether the BCL11B$^{213–560}$ peptide can stimulate the repair of oxidative DNA damage in cells, the peptide was ectopically expressed in RPE1 cells, which express low levels of BCL11B. Since the BCL11B$^{213–560}$ peptide does not contain the nuclear localization signal of BCL11B (77), we added the MYC nuclear localization signal to ensure that the peptide would localize to the nucleus. Measurement of DNA damage by comet assay revealed a decrease in DNA damage in RPE1 cells expressing BCL11B$^{213–560}$ as compared to cells harboring the empty vector (Figure 7A, untreated cells). Moreover, following treatment of cells with H_2O_2, we observed an acceleration of DNA repair in BCL11B$^{213–560}$ expressing cells (Figure 7A). In agreement with the comet assay results, clonogenic assays showed that the BCL11B$^{213–560}$ peptide increased the resistance of RPE1 cells to treatment with 50 and 100 μM H_2O_2 (Figure 7B).

The DNA repair defects caused by BCL11B knockdown are rescued by ectopic expression of the BCL11B$^{213–560}$ fragment

We verified whether ectopic expression of the BCL11B$^{213–560}$ peptide can rescue the DNA repair defect caused by BCL11B knockdown. The increase in the number of genomic abasic sites following BCL11B knockdown was rescued by overexpression of the BCL11B$^{213–560}$ peptide. While we observed a partial rescue in SKES-1 cells (Figure 8A), the rescue was complete in Jurkat cells (Supplementary Figure 4). The increase in genomic DNA damage detected in comet assays at pH 13 and at pH 10 following treatment with the Endo III endonuclease were completely rescued by the BCL11B$^{213–560}$ peptide (Figure 8B). In addition, following treatment with H_2O_2, the delay in DNA repair caused by BCL11B knockdown was rescued by the BCL11B$^{213–560}$ peptide (Figure 8B, recovery after H_2O_2). Immunoblotting analysis did not detect changes in the expression of NTHL1, Pol β, OGG1 and APE1 (Figure 8B). In these experiments, we noticed that BCL11B knockdown caused a decrease in the number of SKES-1 cells. Subsequent experiments failed to detect senescent cells as was previously observed following BCL11A knockdown in breast cancer cells (22). However, upon BCL11B knockdown in SKES-1 cells we observed an increase in the number of early (Annexin V$^+$/PI$^-$) and late (Annexin V$^+$/PI$^+$) apoptotic cells, that was partially rescued by ectopic expression of the BCL11B$^{213–560}$ peptide (Figure 8C). Moreover, CFSE staining on the remaining cells revealed that BCL11B knockdown caused a decrease in proliferation that was partially rescued by the BCL11B$^{213–560}$ peptide (Supplementary Figure 5). That the BCL11B$^{213–560}$ peptide was able to rescue at least partially the apoptosis and proliferation delay phenotypes imparted by *BCL11B* knockdown in sarcoma and T-lymphoma cells demonstrate that the repair function of BCL11B is essential to the fitness of these cancer cells. That the rescue was not complete suggests that the transcriptional activities of BCL11B may also play a critical role in cancer cell fitness.

BCL11B$^{213–560}$ cooperates with RAS to transform primary cells and escape senescence

The acceleration of DNA repair by the BCL11B$^{213–560}$ peptide following treatment with H_2O_2 raised the possibility

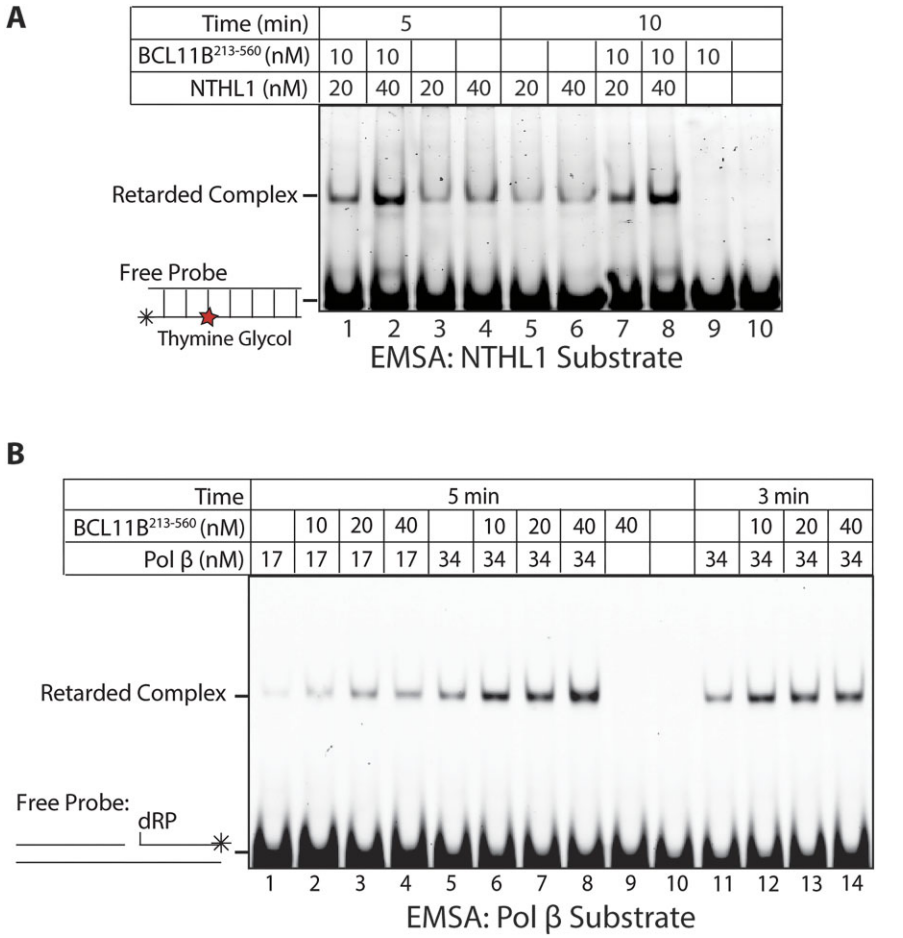

Figure 6. BCL11B stimulates the binding of NTHL1 and Pol β to their substrate. (**A**) Electrophoretic mobility shift assays were performed using oligonucleotides containing a thymine-glycol base. The reactions were performed in the presence of BSA (14.3 μM) and the indicated proteins. (**B**) Electrophoretic mobility shift assays were performed using double-stranded oligonucleotides containing a single-strand nick with a 5′-deoxyribose phosphate. The reactions were performed in the presence of BSA (14.3 μM) and the indicated proteins.

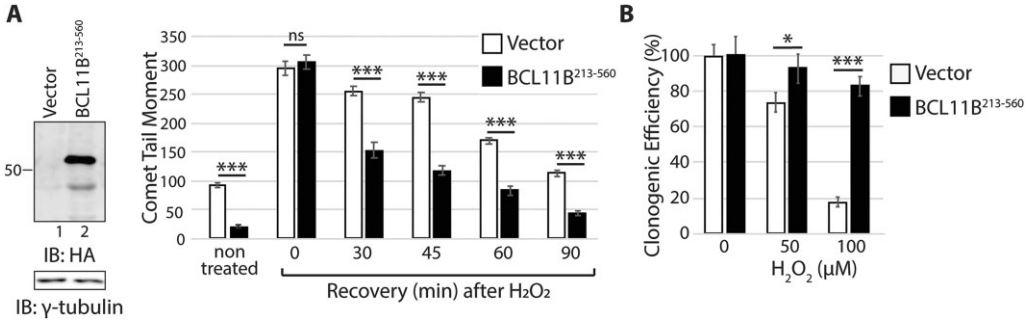

Figure 7. Ectopic Expression of BCL11B$^{213–560}$ accelerates DNA Repair and increases resistance to H_2O_2. (**A**) RPE1 cells expressing the BCL11B$^{213–560}$ peptide were exposed or not to 100 μM H_2O_2 for 20 min and allowed to recover for the indicated time before carrying out single cell gel electrophoresis at pH > 13. Comet tail moments were scored for at least 100 cells per condition. Results are a representative of one of three different experiments. Error bars represent standard error. ***$P < 0.001$; **$P < 0.01$; *$P < 0.05$; Student's *t*-test. (**B**) RPE1 cells expressing the BCL11B$^{213–560}$ peptide were treated with 0, 50 or 100 μM H_2O_2 and submitted to a clonogenic assay. Error bars represent standard error. ***$P < 0.001$; **$P < 0.01$; *$P < 0.05$; Student's *t*-test.

that BCL11B could cooperate with RAS oncogene in cellular transformation (78). One obstacle to RAS-transformation is the increased production of reactive oxygen species that cause oxidative DNA damage and, ultimately, cellular senescence (79–81). To test whether the DNA repair activity of BCL11B may cooperate with RAS, we performed co-infections into the IMR90 human primary fibroblastic cells to express the HRAS^{G12V} oncogene together with BCL11B$^{213–560}$ or the empty vector (Figure 9A). The number of soft agar colonies was increased when HRAS^{G12V} was expressed with BCL11B$^{213–560}$ (Figure 9B). As expected, the HRAS oncogene caused an increase in DNA damage measured by comet

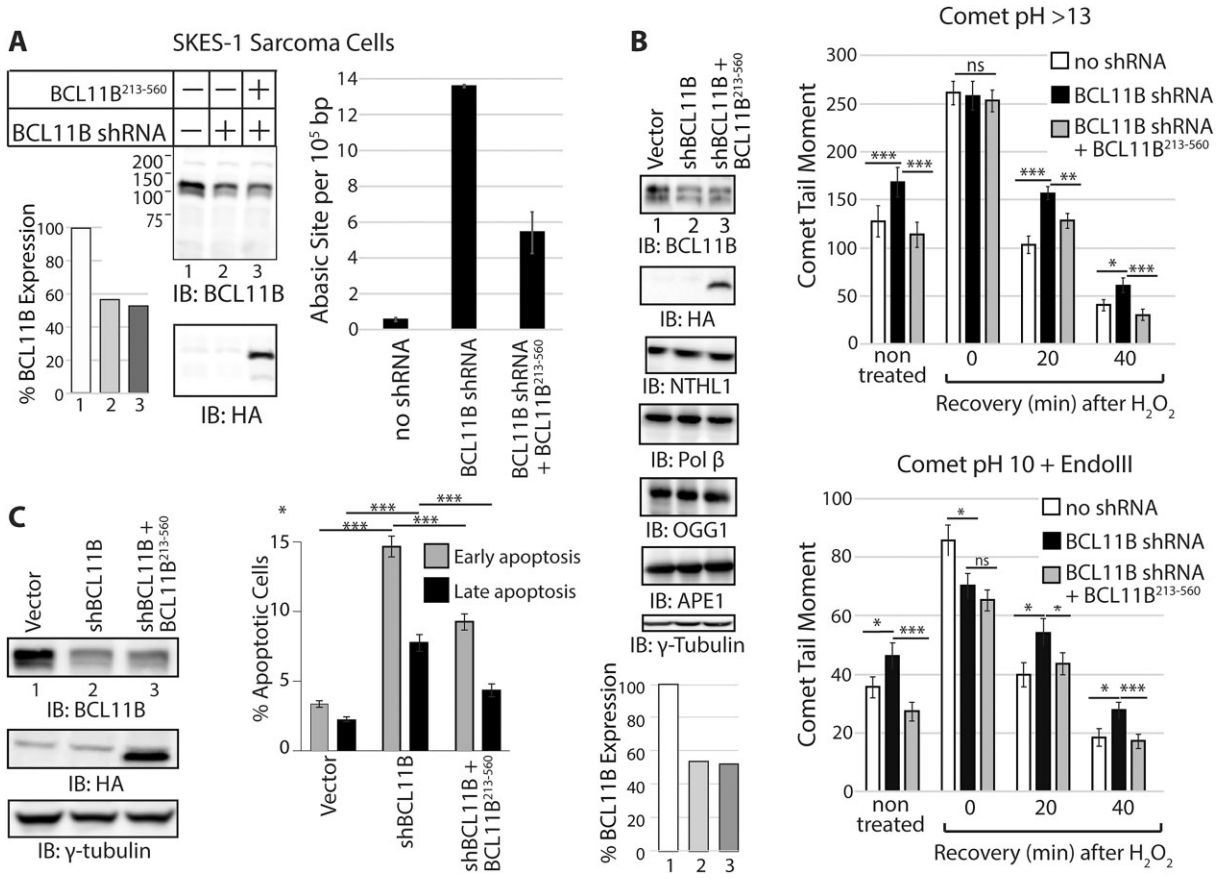

Figure 8. The DNA repair defects caused by BCL11B knockdown are rescued by ectopic expression of the BCL11B$^{213–560}$ fragment. (**A**) SKES-1 sarcoma cells were infected with a lentiviral vector expressing BCL11B shRNA. One batch of cells was co-infected with a lentivirus expressing the BCL11B$^{213–560}$ recombinant protein. Protein extracts were processed for immunoblotting analysis (left), while genomic DNA was purified and abasic sites were quantified using an aldehyde-reactive probe (right). (**B**) SKES-1 sarcoma cells were infected with a lentiviral vector expressing BCL11B shRNA. One batch of cells was co-infected with a lentivirus expressing the BCL11B$^{213–560}$ recombinant protein. Cells were exposed or not to 50 μM H_2O_2 for 20 min and allowed to recover for the indicated time before carrying out single cell gel electrophoresis at pH > 13, or at pH 10 after treatment of cells with the Endo III DNA glycosylase. Comet tail moments were scored for at least 100 cells per condition. Results are a representative one of three different experiments. Error bars represent standard error. ***$P < 0.001$; **$P < 0.01$; *$P < 0.05$; Student's *t*-test. (**C**) SKES-1 sarcoma cells were infected with a lentiviral vector expressing BCL11B shRNA. One batch of cells was co-infected with a lentivirus expressing the BCL11B$^{213–560}$ recombinant protein. On day 4, cells were stained for annexin V and propidium iodide and analyzed by FACS. A summary of the results is presented as a histogram.

assay, but this increase was prevented by co-expression with the BCL11B$^{213–560}$ fragment (Figure 9C). The increase in DNA damage caused by the HRAS oncogene was associated with a block to cell proliferation as monitored by cell counting (Figure 9D) and an increase in the number of senescent cells as measured by β-galactosidase activity (Figure 9E). Proliferation was rescued by co-expression of the BCL11B$^{213–560}$ peptide (Figure 9D). The number of senescent cells was also reduced by co-expression of the BCL11B$^{213–560}$ peptide (Figure 9E). We conclude that the DNA repair function of BCL11B helps primary cells in which the RAS pathway becomes permanently activated to avoid cellular senescence and continue to proliferate.

Inactivation of one BCL11B allele causes an increase in spontaneous and radiation-induced mutation rates

We then used the CRISPR/Cas approach to generate clones of TK6 lymphoblastoid cells in which one allele of BCL11B is inactivated. We chose to transfect the CRISPR/Cas protein instead of an expression vector to increase the probability of inactivating only one of the two alleles. Three different single-guide RNAs were designed. Following optimization, we isolated and analyzed clones generated with different guide RNAs. Two clones that harbored one wild type allele and a frameshift mutation in the other allele were chosen for further investigation (Figure 10A). The fluctuation assay was performed to measure the spontaneous and radiation-induced mutation rates within the *HPRT* gene. Since there is only one copy of the *HPRT* gene and it is easy to select for HPRT-minus and HPRT-positive cells, measuring inactivation of the *HPRT* gene is a standard method to measure mutation rates (82). The fluctuation assay was devised by Luria and Delbruck to test the hypothesis that mutations occur spontaneously in bacteria (83). The assay was later adapted to the measurement of mutation rates in mammalian cells (69,70). Briefly, for the spontaneous mutation rate, following selection against *HPRT*-minus cells 24 independent cultures were started each with 100 cells and were allowed to proliferate until they reached 8 million cells at which point 6-thioguanine was added to the medium to select for *HPRT*-minus cells. The number of cultures with some HPRT-minus cells served to calculate the mutation rate according to the equations

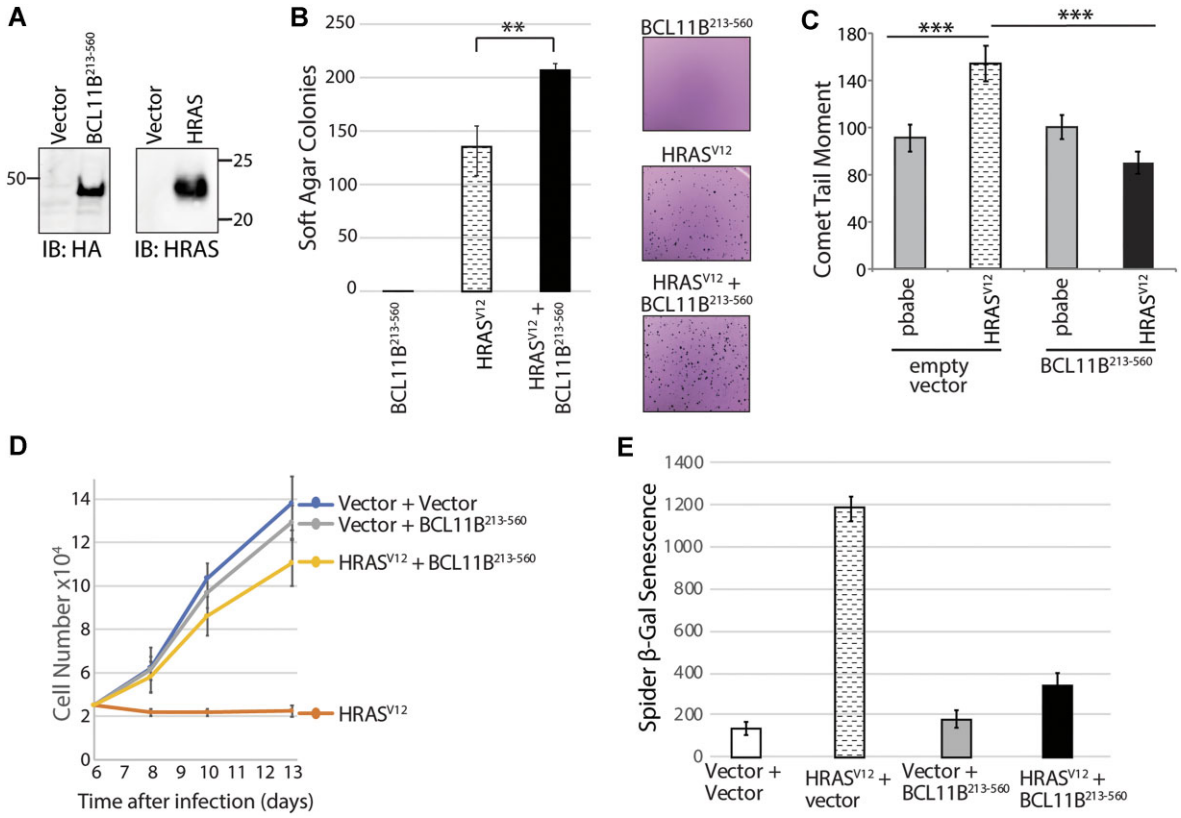

Figure 9. BCL11B cooperates with RAS to transform primary cells and escape senescence IMR90 primary fibroblastic cells were infected with retroviruses expressing either HRAS alone or HRAS and BCL11B$^{213\text{-}560}$, as indicated. (**A**) Total cell extracts were analyzed by immunoblotting with the indicated antibodies. (**B**) On day 2, cells were plated in soft agar and colonies were counted after 2 weeks $***P < 0.001$; $**P < 0.01$; $*P < 0.05$; Student's *t*-test. (**C**) IMR90 cells were selected for 5 days with puromycin, cells were then submitted to single cell gel electrophoresis at pH > 13. Comet tail moments were scored for at least 100 cells per condition. Results are a representative of one of three different experiments. Error bars represent standard error. $***P < 0.001$; $**P < 0.01$; $*P < 0.05$; Student's *t*-test. (**D**) On day 6, cells were plated at a density of 25 000 cells in a 60 mm plate and allowed to proliferate. Cells were counted on the indicated days. (**E**) β-Gal associated senescence was measured on 10 000 cells 6 days after infection with vectors expressing HRAS or HRAS and BCL11B$^{213–560}$. Values were normalized to the value of empty vector. Error bars represent standard error. $***P < 0.001$; $**P < 0.01$; $*P < 0.05$; Student's *t*-test.

detailed in Materials and Methods (69,70). We observed spontaneous mutation rates of 3.1×10^{-8} for the parental TK6 cells and of 17×10^{-8} and 13×10^{-8} for the heterozygous clones 101 and 203, respectively (Figure 10B and C). After 1.5 Gy irradiation, the mutation rates increased to 5.6×10^{-7} for the parental TK6 cells and to 13×10^{-7} and 14×10^{-7} for the heterozygous clones 101 and 203, respectively (Figure 10B and C). Thus, inactivation of one BCL11B allele caused an increase in spontaneous mutation rates of 5.5- and 4.4-fold in clones 101 and 203, respectively (Figure 10B and C). The increase in radiation-induced mutation rates was 2.3- and 2.6-fold in clones 101 and 203, respectively (Figure 10B and C).

Discussion

Prior findings demonstrated that CUT domain proteins can stimulate the enzymatic activities of OGG1 but not of other glycosylases of the base excision repair pathway. Hence, we hypothesized that other DNA glycosylases may interact with distinct accessory factors, and therefore aimed to identify accessory factors for NTHL1, the main glycosylase that removes oxidized pyrimidines. Proximity biotinylation with a NTHL1-BirA* protein identified BCL11B, a protein that functions as a transcription factor (22). The increase in genomic DNA damage and the decrease in DNA repair upon BCL11B knockdown in SKES-1 and A673 sarcoma cells and in Jurkat T lymphoma cells indicated that BCL11B is required at some level for efficient DNA repair (Figure 2 and Supplementary Figure 1). In particular, the increase in oxidized bases and abasic sites pointed to a defect in base excision repair. As we did not observe any change in the expression of base excision repair proteins upon BCL11B knockdown (Figures 2C and 8B), we verified whether BCL11B could play a direct role in DNA repair. The recruitment of BCL11B to laser microirradiation-induced DNA damage is consistent with a direct role in DNA repair, however, we cannot exclude the possibility that this recruitment may simply be the consequence of chromatin opening at the sites of DNA damage making it easier for a transcription factor to bind to DNA (Figure 3). Results from *in vitro* DNA repair assays showed that BCL11B can stimulate the enzymatic activities of two enzymes of the base excision repair pathway, NTHL1 and Pol β (Figures 4 and 5). Moreover, structure-function analysis revealed that the BCL11B region required and sufficient to stimulate DNA repair enzymatic activities, BCL11B$^{213–560}$, does not include the C-terminal zinc fingers that are needed for specific DNA binding nor the N-terminal domains involved in transcriptional regulation and dimerization (Figures 4, 5 and Supplementary Figure 2) (60,77). Importantly, ectopic expression of the BCL11B$^{213–560}$

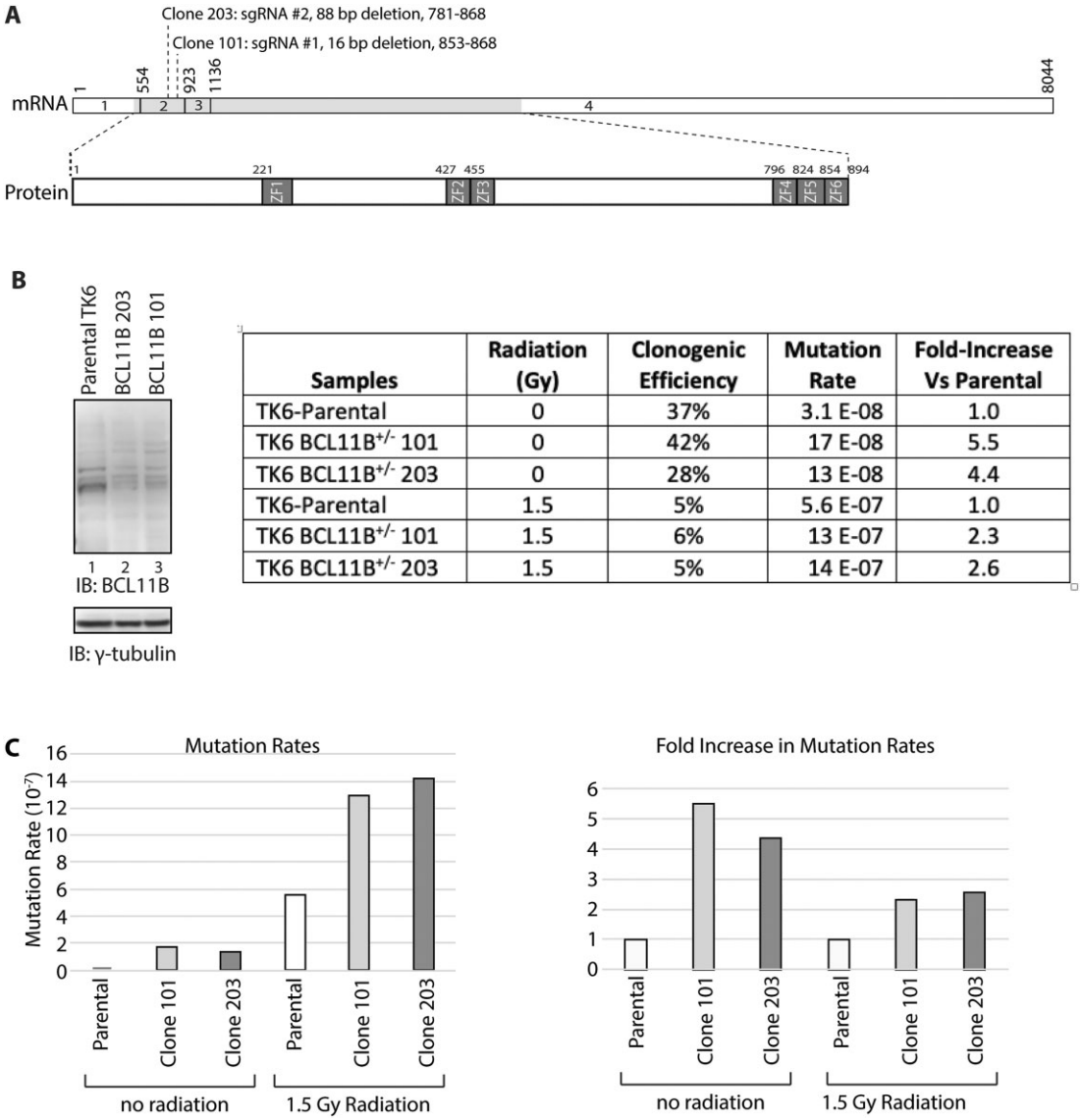

Samples	Radiation (Gy)	Clonogenic Efficiency	Mutation Rate	Fold-Increase Vs Parental
TK6-Parental	0	37%	3.1 E-08	1.0
TK6 BCL11B$^{+/-}$ 101	0	42%	17 E-08	5.5
TK6 BCL11B$^{+/-}$ 203	0	28%	13 E-08	4.4
TK6-Parental	1.5	5%	5.6 E-07	1.0
TK6 BCL11B$^{+/-}$ 101	1.5	6%	13 E-07	2.3
TK6 BCL11B$^{+/-}$ 203	1.5	5%	14 E-07	2.6

Figure 10. Inactivation of one BCL11B allele causes an increase in spontaneous and radiation-induced mutation rates. (**A**) Diagrammatic representation of BCL11B mRNA and protein. The boxes represent the four exons, while the shaded area indicates the coding sequences. Above the mRNA map are shown the positions of the mutations in clones 203 and 101, which were respectively generated using sgRNA #2 and #1. (**B**) Fluctuation assays were performed to measure the mutation rates within the *HPRT* gene in two independent clones of BCL11B$^{+/-}$ heterozygous TK6 cells as well as in parental TK6 cells. A brief description of the fluctuation assay is provided in Materials and Methods. The table shows the clonogenic efficiencies, mutation rates and fold-increases relative to parental cells. (**C**) The histogram on the left shows the mutation rates, the histogram on the right shows the fold increases relative to parental cells.

peptide in RPE1 cells led to a reduction of genomic DNA damage and acceleration of DNA repair following treatment with H_2O_2 (Figure 7). Moreover, the BCL11B$^{213–560}$ peptide was able to rescue the DNA repair defects resulting from BCL11B knockdown (Figure 8A, B and Supplementary Figure 4). While ectopic expression of the BCL11B$^{213–560}$ peptide rescued DNA repair defects, it only partially rescued the increase in the number of apoptotic cells caused by BCL11B knockdown in SKES-1 cells (Figure 8C). This finding suggests that the transcriptional functions of BCL11B are also required for the fitness of SKES-1 cells. Altogether these results demonstrate that in addition to its transcriptional functions BCL11B can also carry out biochemical activities that are directly involved in DNA repair. These findings provide a mechanistic explanation for previous observations linking *BCL11B* overexpression and resistance to genotoxic treatments (42,43). It is also likely that the DNA repair function of BCL11B is particularly important in stem/progenitor cells where it is expressed.

Our results showed that the BCL11B$^{213–560}$ peptide was able to enhance the binding of NTHL1 and Pol β to their respective substrates. This biochemical activity probably explains how BCL11B can stimulate the enzymatic activities of these enzymes. The exact mechanism by which BCL11B increases the binding of these enzymes to their substrates remains to be investigated. We did not observe that the BCL11B$^{213–560}$ peptide formed a retarded complex with either probe, however, we cannot exclude that a very weak or short-lived interaction can occur that helps the BER enzymes recognize their substrates. Alternatively, we would have to envision that the interaction between BCL11B and the enzymes

triggers a conformational change that makes the enzymes bind more rapidly to their substrate.

The role of BCL11B as an accessory factor stimulating both NTHL1 and Pol β is coherent. Indeed, since NTHL1 is also endowed with an AP-lyase activity, it is important that the resulting single-strand break be rapidly resolved by BER enzymes acting downstream in the pathway. Earlier studies have previously revealed the importance of maintaining a proper balance in the enzymatic activities of BER enzymes (84). For example, cancer cells can be rendered more susceptible to the killing effect of the mono-alkylating agent temozolomide by increasing expression of methylpurine DNA glycosylase or alternatively, by decreasing Pol β expression. The resulting imbalance in base excision repair leads to the accumulation of cytotoxic single-strand breaks with 5′-deoxyribose phosphate (75,85). In a similar manner, the stimulation of OGG1 or NTHL1 enzymatic activities by accessory factors in cancer cells that exhibit high levels of reactive oxygen species could potentially produce cytotoxic single-strand breaks that are deleterious to cell viability unless the increased glycosylase activity is matched with an increase in Pol β activity.

The finding that ectopic expression of $BCL11B^{213–560}$ in RPE1, SKES-1 and Jurkat cells leads to a reduction in genomic DNA damage suggested that the DNA repair function of BCL11B may cooperate with RAS in cell transformation since one roadblock to cellular transformation is the senescence response triggered by excess oxidative DNA damage. Indeed, in the RAS-transformation assay, we observed that $BCL11B^{213–560}$ cooperates with RAS to transform IMR90 primary fibroblast cells in a soft agar assay (Figure 9B). This was associated with a lower level of DNA damage, an increase in cell proliferation and a reduction in the number of senescent cells (Figure 9C–E). Similar observations had been made with the CUX1 and BCL11A transcription factors that also function as BER accessory factors (19,22). Overall, these findings show that the upregulation of BER accessory factors can be exploited by cancer cells to avoid senescence and continue to proliferate despite producing excess levels of reactive oxygen species.

Many cancer cells produce an excess of reactive oxygen species (ROS) that cause oxidative DNA damage and, ultimately, cellular senescence (79–81). This has been documented not only in tissue culture and mouse models (86–88), but also in premalignant human colon adenomas (89–91), as well as in human benign lesions caused by the $BRAF^{V600E}$ mutation (92) or NF1 inactivation (93). In this context, cellular senescence has been deemed a tumor suppression mechanism (94). Unfortunately, cancer cells can sometimes adapt and continue to proliferate despite producing high levels of ROS. One mechanism of adaptation that has been firmly documented is through the increased expression of antioxidants, notably following inactivation of the *KEAP1* tumor suppressor gene, an event observed in 15–30% of cancers (95–98). A different mechanism of adaptation has recently emerged. A synthetic lethality screen had revealed that RAS-transformed cells are significantly more dependent on an efficient BER pathway than are normal cells (99). Subsequent studies identified a number of transcription factors that function as BER accessory factors and are overexpressed in cancer: CUX1, CUX2, SATB1 and BCL11A (16,18,19,21,22,100). Strikingly, the DNA repair activity of these accessory factors was shown to enable cancer cells to avoid cellular senescence and continue to proliferate in spite of elevated ROS levels (16,18,19,21,22,100). This led us to propose a second mechanism of adaptation to elevated ROS production: some cancer cells can adapt by increasing their capacity to repair oxidative DNA damage. This can be achieved through increased expression of enzymes of the base excision repair (BER) pathway, as well as BER accessory factors (101,102). Results from the present study add yet another BER accessory factor, BCL11B, whose DNA repair function is exploited by some cancer cells to ensure their survival.

From studies in humans and mice, BCL11B has been genetically characterized as a haploinsufficient tumor suppressor gene. Monoallelic *BCL11B* deletions or inactivating point mutations have been reported in 9–16% of human T-cell acute lymphoblastic leukemias (27–29). In mice, the study of γ-ray induced mouse thymic lymphomas led to the identification of *Bcl11B*, which was first termed radiation-induced tumor suppressor gene 1 (Rit1) (23–26). Subsequent studies showed that heterozygous *Bcl11B* mice exhibit higher incidence of thymic lymphomas after γ-radiation or crossing with p53 heterozygous mice (30–32). Mechanistically, it has been challenging to explain how the same transcription factor can function as an oncogene and a tumor suppressor gene in the same cell lineage. We showed here that two independent clones of TK6 lymphoblastoid cells, in which one BCL11B allele has been inactivated, exhibit higher spontaneous and radiation-induced mutation rates (Figure 10). As $BCL11B^{+/-}$ heterozygous cells accumulate mutations at a faster rate, the probability that they acquire cancer driver mutations is increased. Thus, the DNA repair functions of BCL11B protect certain cells against the acquisition of mutations. We consider likely that the stimulation of Pol β enzymatic activities is the biochemical activity of BCL11B that explains its role as a haploinsufficient tumor suppressor. Indeed, somatic mutations in the *Pol β* gene were found in approximately 30% of tumours analyzed (103). One mutant in particular, Pol $β^{K289M}$, caused a 2.5-fold increase in mutation frequency and was shown to induce a transformed phenotype in mouse cells (104).

The *BCL11A* and *BCL11B* genes have arisen recently during evolution such that the two proteins are very similar. Indeed, our structure-function analysis, *in vitro* DNA repair assays and cell-based assays revealed that the two proteins fulfill similar functions in base excision repair. Our results also showed that BCL11A and BCL11B are required for the survival of the cancer cells in which they are overexpressed. Yet, only the *BCL11B* gene has been characterized as a haploinsufficient tumor suppressor gene. We believe one explanation has to do with the particular cell types in which each of these proteins is expressed. Specifically, T cells are a type of cells that must proliferate and expand very rapidly upon immune stimulation. Moreover, T cells are often present at sites of inflammation. The physiological functions of T cells may require a more efficient base excision repair pathway in which BER accessory factors become important. These properties could make T cells more susceptible to the acquisition of mutations when the expression of the BCL11B accessory factor is reduced. In contrast, the DNA repair functions of BCL11A do not appear to be required in normal cells.

To our knowledge, only the *CUX1* and *BCL11B* genes have been characterized genetically both as oncogenes and haplo-insufficient tumor suppressor genes (27–29,105). Results from the present study demonstrate that in addition to its function as a transcription factor, the BCL11B protein also plays a direct role in base excision repair. Notably, the

findings that reduced BCL11B expression causes an increase in spontaneous and radiation-induced mutation rates, and that increased BCL11B expression in cancer cells accelerates the repair of oxidative DNA damage provide a mechanistic understanding for the paradoxical roles of BCL11B in cancer.

Data availability

The data underlying this article are available in the article and in its online supplementary material.

Supplementary data

Supplementary Data are available at NAR Online.

Acknowledgements

Image processing and analysis was performed in the McGill University Advanced BioImaging Facility; flow cytometry experiments at the Flow Cytometry and Cell Sorting Facility.

Funding

Canadian Institutes of Health Research [MOP-391532]; National Science and Engineering Council [RGPIN-2016-05155 to A.N.]. Funding for open access charge: Research grants.

Conflict of interest statement

None declared.

References

1. Bauer,N.C., Corbett,A.H. and Doetsch,P.W. (2015) The current state of eukaryotic DNA base damage and repair. *Nucleic Acids Res.*, **43**, 10083–10101.
2. Dianov,G.L. and Hubscher,U. (2013) Mammalian base excision repair: the forgotten archangel. *Nucleic Acids Res.*, **41**, 3483–3490.
3. Demple,B. and Harrison,L. (1994) Repair of oxidative damage to DNA: enzymology and biology. *Annu. Rev. Biochem.*, **63**, 915–948.
4. Hegde,M.L., Hazra,T.K. and Mitra,S. (2008) Early steps in the DNA base excision/single-strand interruption repair pathway in mammalian cells. *Cell Res.*, **18**, 27–47.
5. Weinfeld,M., Mani,R.S., Abdou,I., Aceytuno,R.D. and Glover,J.N. (2011) Tidying up loose ends: the role of polynucleotide kinase/phosphatase in DNA strand break repair. *Trends Bioc. Sci.*, **36**, 262–271.
6. Demple,B. and Sung,J.S. (2005) Molecular and biological roles of Ape1 protein in mammalian base excision repair. *DNA Repair (Amst.)*, **4**, 1442–1449.
7. Wiederhold,L., Leppard,J.B., Kedar,P., Karimi-Busheri,F., Rasouli-Nia,A., Weinfeld,M., Tomkinson,A.E., Izumi,T., Prasad,R., Wilson,S.H., *et al.* (2004) AP endonuclease-independent DNA base excision repair in human cells. *Mol. Cell*, **15**, 209–220.
8. Allinson,S.L. and Dianov,G.L. (2001) DNA polymerase beta is the major dRP lyase involved in repair of oxidative base lesions in DNA by mammalian cell extracts. *EMBO J.*, **20**, 6919–6926.
9. Horton,J.K., Prasad,R., Hou,E. and Wilson,S.H. (2000) Protection against methylation-induced cytotoxicity by DNA polymerase beta-dependent long patch base excision repair. *J. Biol. Chem.*, **275**, 2211–2218.
10. Ba,X. and Boldogh,I. (2018) 8-Oxoguanine DNA glycosylase 1: beyond repair of the oxidatively modified base lesions. *Redox. Biol.*, **14**, 669–678.
11. Das,S., Chattopadhyay,R., Bhakat,K.K., Boldogh,I., Kohno,K., Prasad,R., Wilson,S.H. and Hazra,T.K. (2007) Stimulation of NEIL2-mediated oxidized base excision repair via YB-1 interaction during oxidative stress. *J Biol. Chem.*, **282**, 28474–28484.
12. Hegde,M.L., Banerjee,S., Hegde,P.M., Bellot,L.J., Hazra,T.K., Boldogh,I. and Mitra,S. (2012) Enhancement of NEIL1 protein-initiated oxidized DNA base excision repair by heterogeneous nuclear ribonucleoprotein U (hnRNP-U) via direct interaction. *J. Biol. Chem.*, **287**, 34202–34211.
13. Prasad,R., Liu,Y., Deterding,L.J., Poltoratsky,V.P., Kedar,P.S., Horton,J.K., Kanno,S., Asagoshi,K., Hou,E.W., Khodyreva,S.N., *et al.* (2007) HMGB1 is a cofactor in mammalian base excision repair. *Mol. Cell*, **27**, 829–841.
14. Charles Richard,J.L., Shukla,M.S., Menoni,H., Ouararhni,K., Lone,I.N., Roulland,Y., Papin,C., Ben Simon,E., Kundu,T., Hamiche,A., *et al.* (2016) FACT assists base excision repair by boosting the remodeling activity of RSC. *PLos Genet.*, **12**, e1006221.
15. Zhou,J., Ahn,J., Wilson,S.H. and Prives,C. (2001) A role for p53 in base excision repair. *EMBO J.*, **20**, 914–923.
16. Kaur,S., Coulombe,Y., Ramdzan,Z.M., Leduy,L., Masson,J.Y. and Nepveu,A. (2016) Special AT-rich sequence-binding protein 1 (SATB1) functions as an accessory factor in base excision repair. *J. Biol. Chem.*, **291**, 22769–22780.
17. Ramdzan,Z.M., Pal,R., Kaur,S., Leduy,L., Berube,G., Davoudi,S., Vadnais,C. and Nepveu,A. (2015) The function of CUX1 in oxidative DNA damage repair is needed to prevent premature senescence of mouse embryo fibroblasts. *Oncotarget*, **6**, 3613–3626.
18. Pal,R., Ramdzan,Z.M., Kaur,S., Duquette,P.M., Marcotte,R., Leduy,L., Davoudi,S., Lamarche-Vane,N., Iulianella,A. and Nepveu,A. (2015) CUX2 Functions As an accessory factor in the repair of oxidative DNA damage. *J. Biol. Chem.*, **290**, 22520–22531.
19. Ramdzan,Z.M., Vadnais,C., Pal,R., Vandal,G., Cadieux,C., Leduy,L., Davoudi,S., Hulea,L., Yao,L., Karnezis,A.N., *et al.* (2014) RAS transformation requires CUX1-dependent repair of oxidative DNA damage. *PLoS Biol.*, **12**, e1001807
20. Ramdzan,Z.M., Vickridge,E., Li,L., Faraco,C.C.F., Djerir,B., Leduy,L., Marechal,A. and Nepveu,A. (2021) CUT domains stimulate pol beta enzymatic activities to accelerate completion of base excision repair. *J. Mol. Biol.*, **433**, 166806.
21. Kaur,S., Ramdzan,Z.M., Guiot,M.C., Li,L., Leduy,L., Ramotar,D., Sabri,S., Abdulkarim,B. and Nepveu,A. (2018) CUX1 Stimulates APE1 enzymatic activity and increases the resistance of glioblastoma cells to the mono-alkylating agent, temozolomide. *Neuro-oncol.*, **20**, 484–493.
22. Vickridge,E., Faraco,C.C.F., Tehrani,P.S., Ramdzan,Z.M., Djerir,B., Rahimian,H., Leduy,L., Maréchal,A., Gingras,A.C. and Nepveu,A. (2022) The DNA repair function of BCL11A suppresses senescence and promotes continued proliferation of triple-negative breast cancer cells. *NAR Cancer*, **4**, zcac028.
23. Wakabayashi,Y., Watanabe,H., Inoue,J., Takeda,N., Sakata,J., Mishima,Y., Hitomi,J., Yamamoto,T., Utsuyama,M., Niwa,O., *et al.* (2003) Bcl11b is required for differentiation and survival of alphabeta T lymphocytes. *Nat. Immunol.*, **4**, 533–539.
24. Wakabayashi,Y., Inoue,J., Takahashi,Y., Matsuki,A., Kosugi-Okano,H., Shinbo,T., Mishima,Y., Niwa,O. and Kominami,R. (2003) Homozygous deletions and point mutations of the Rit1/Bcl11b gene in gamma-ray induced mouse thymic lymphomas. *Biochem. Biophys. Res. Commun.*, **301**, 598–603.
25. Sakata,J., Inoue,J., Ohi,H., Kosugi-Okano,H., Mishima,Y., Hatakeyama,K., Niwa,O. and Kominami,R. (2004) Involvement of V(D)J recombinase in the generation of intragenic deletions in the Rit1/Bcl11b tumor suppressor gene in gamma-ray-induced

thymic lymphomas and in normal thymus of the mouse. *Carcinogenesis*, **25**, 1069–1075.
26. Matsumoto,Y., Kosugi,S., Shinbo,T., Chou,D., Ohashi,M., Wakabayashi,Y., Sakai,K., Okumoto,M., Mori,N., Aizawa,S., *et al.* (1998) Allelic loss analysis of gamma-ray-induced mouse thymic lymphomas: two candidate tumor suppressor gene loci on chromosomes 12 and 16. *Oncogene*, **16**, 2747–2754.
27. Gutierrez,A., Kentsis,A., Sanda,T., Holmfeldt,L., Chen,S.C., Zhang,J., Protopopov,A., Chin,L., Dahlberg,S.E., Neuberg,D.S., *et al.* (2011) The BCL11B tumor suppressor is mutated across the major molecular subtypes of T-cell acute lymphoblastic leukemia. *Blood*, **118**, 4169–4173.
28. De Keersmaecker,K., Real,P.J., Gatta,G.D., Palomero,T., Sulis,M.L., Tosello,V., Van Vlierberghe,P., Barnes,K., Castillo,M., Sole,X., *et al.* (2010) The TLX1 oncogene drives aneuploidy in T cell transformation. *Nat. Med.*, **16**, 1321–1327.
29. Przybylski,G.K., Dik,W.A., Wanzeck,J., Grabarczyk,P., Majunke,S., Martin-Subero,J.I., Siebert,R., Dolken,G., Ludwig,W.D., Verhaaf,B., *et al.* (2005) Disruption of the BCL11B gene through inv(14)(q11.2q32.31) results in the expression of BCL11B-TRDC fusion transcripts and is associated with the absence of wild-type BCL11B transcripts in T-ALL. *Leukemia*, **19**, 201–208.
30. Kamimura,K., Mishima,Y., Obata,M., Endo,T., Aoyagi,Y. and Kominami,R. (2007) Lack of Bcl11b tumor suppressor results in vulnerability to DNA replication stress and damages. *Oncogene*, **26**, 5840–5850.
31. Ohi,H., Mishima,Y., Kamimura,K., Maruyama,M., Sasai,K. and Kominami,R. (2007) Multi-step lymphomagenesis deduced from DNA changes in thymic lymphomas and atrophic thymuses at various times after gamma-irradiation. *Oncogene*, **26**, 5280–5289.
32. Kominami,R. (2012) Role of the transcription factor Bcl11b in development and lymphomagenesis. *Proc. Jpn. Acad. Ser. B. Phys. Biol. Sci.*, **88**, 72–87.
33. Gu,X., Wang,Y., Zhang,G., Li,W. and Tu,P. (2013) Aberrant expression of BCL11B in mycosis fungoides and its potential role in interferon-induced apoptosis. *J. Dermatol.*, **40**, 596–605.
34. Ganguli-Indra,G., Wasylyk,C., Liang,X., Millon,R., Leid,M., Wasylyk,B., Abecassis,J. and Indra,A.K. (2009) CTIP2 expression in human head and neck squamous cell carcinoma is linked to poorly differentiated tumor status. *PLoS One*, **4**, e5367.
35. Wiles,E.T., Lui-Sargent,B., Bell,R. and Lessnick,S.L. (2013) BCL11B is up-regulated by EWS/FLI and contributes to the transformed phenotype in Ewing sarcoma. *PLoS One*, **8**, e59369.
36. Oshiro,A., Tagawa,H., Ohshima,K., Karube,K., Uike,N., Tashiro,Y., Utsunomiya,A., Masuda,M., Takasu,N., Nakamura,S., *et al.* (2006) Identification of subtype-specific genomic alterations in aggressive adult T-cell leukemia/lymphoma. *Blood*, **107**, 4500–4507.
37. Liao,C.K., Fang,K.M., Chai,K., Wu,C.H., Ho,C.H., Yang,C.S. and Tzeng,S.F. (2016) Depletion of B cell CLL/lymphoma 11B gene expression represses glioma cell growth. *Mol. Neurobiol.*, **53**, 3528–3539.
38. Grabarczyk,P., Przybylski,G.K., Depke,M., Volker,U., Bahr,J., Assmus,K., Broker,B.M., Walther,R. and Schmidt,C.A. (2007) Inhibition of BCL11B expression leads to apoptosis of malignant but not normal mature T cells. *Oncogene*, **26**, 3797–3810.
39. Huang,X., Chen,S., Shen,Q., Chen,S., Yang,L., Grabarczyk,P., Przybylski,G.K., Schmidt,C.A. and Li,Y. (2011) Down regulation of BCL11B expression inhibits proliferation and induces apoptosis in malignant T cells by BCL11B-935-siRNA. *Hematology*, **16**, 236–242.
40. Baldauf,M.C., Orth,M.F., Dallmayer,M., Marchetto,A., Gerke,J.S., Rubio,R.A., Kiran,M.M., Musa,J., Knott,M.M.L., Ohmura,S., *et al.* (2018) Robust diagnosis of Ewing sarcoma by immunohistochemical detection of super-enhancer-driven EWSR1-ETS targets. *Oncotarget*, **9**, 1587–1601.
41. Orth,M.F., Holting,T.L.B., Dallmayer,M., Wehweck,F.S., Paul,T., Musa,J., Baldauf,M.C., Surdez,D., Delattre,O., Knott,M.M.L., *et al.* (2020) High specificity of BCL11B and GLG1 for EWSR1-FLI1 and EWSR1-ERG positive ewing sarcoma. *Cancers*, **12**, 644–661.
42. Zweier-Renn,L.A., Riz,I., Hawley,T.S. and Hawley,R.G. (2013) The DN2 myeloid-T (DN2mt) progenitor is a target cell for leukemic transformation by the TLX1 oncogene. *J. Bone Marrow Res.*, **1**, 105–131.
43. Grabarczyk,P., Nahse,V., Delin,M., Przybylski,G., Depke,M., Hildebrandt,P., Volker,U. and Schmidt,C.A. (2010) Increased expression of bcl11b leads to chemoresistance accompanied by G1 accumulation. *PLoS One*, **5**, e12532.
44. Avram,D., Fields,A., Pretty On Top,K., Nevrivy,D.J., Ishmael,J.E. and Leid,M. (2000) Isolation of a novel family of C(2)H(2) zinc finger proteins implicated in transcriptional repression mediated by chicken ovalbumin upstream promoter transcription factor (COUP-TF) orphan nuclear receptors. *J. Biol. Chem.*, **275**, 10315–10322.
45. Zhang,L.J., Vogel,W.K., Liu,X., Topark-Ngarm,A., Arbogast,B.L., Maier,C.S., Filtz,T.M. and Leid,M. (2012) Coordinated regulation of transcription factor Bcl11b activity in thymocytes by the mitogen-activated protein kinase (MAPK) pathways and protein sumoylation. *J. Biol. Chem.*, **287**, 26971–26988.
46. Topark-Ngarm,A., Golonzhka,O., Peterson,V.J., Barrett,B., Martinez,B., Crofoot,K., Filtz,T.M. and Leid,M. (2006) CTIP2 associates with the NuRD complex on the promoter of p57KIP2, a newly identified CTIP2 target gene. *J. Biol. Chem.*, **281**, 32272–32283.
47. Cismasiu,V.B., Paskaleva,E., Suman Daya,S., Canki,M., Duus,K. and Avram,D. (2008) BCL11B is a general transcriptional repressor of the HIV-1 long terminal repeat in T lymphocytes through recruitment of the NuRD complex. *Virology*, **380**, 173–181.
48. Cismasiu,V.B., Ghanta,S., Duque,J., Albu,D.I., Chen,H.M., Kasturi,R. and Avram,D. (2006) BCL11B participates in the activation of IL2 gene expression in CD4+ T lymphocytes. *Blood*, **108**, 2695–2702.
49. Cismasiu,V.B., Adamo,K., Gecewicz,J., Duque,J., Lin,Q. and Avram,D. (2005) BCL11B functionally associates with the NuRD complex in T lymphocytes to repress targeted promoter. *Oncogene*, **24**, 6753–6764.
50. Dubuissez,M., Loison,I., Paget,S., Vorng,H., Ait-Yahia,S., Rohr,O., Tsicopoulos,A. and Leprince,D. (2016) Protein kinase C-mediated phosphorylation of BCL11B at serine 2 negatively regulates its interaction with NuRD complexes during CD4+ T-cell activation. *Mol. Cell. Biol.*, **36**, 1881–1898.
51. Liu,P., Li,P. and Burke,S. (2010) Critical roles of Bcl11b in T-cell development and maintenance of T-cell identity. *Immunol. Rev.*, **238**, 138–149.
52. Holmes,T.D., Pandey,R.V., Helm,E.Y., Schlums,H., Han,H., Campbell,T.M., Drashansky,T.T., Chiang,S., Wu,C.Y., Tao,C., *et al.* (2021) The transcription factor Bcl11b promotes both canonical and adaptive NK cell differentiation. *Sci. Immunol.*, **6**, 9801–9817.
53. Drashansky,T.T., Helm,E., Huo,Z., Curkovic,N., Kumar,P., Luo,X., Parthasarathy,U., Zuniga,A., Cho,J.J., Lorentsen,K.J., *et al.* (2019) Bcl11b prevents fatal autoimmunity by promoting treg cell program and constraining innate lineages in treg cells. *Sci. Adv.*, **5**, eaaw0480.
54. Hosokawa,H., Romero-Wolf,M., Yui,M.A., Ungerback,J., Quiloan,M.L.G., Matsumoto,M., Nakayama,K.I., Tanaka,T. and Rothenberg,E.V. (2018) Bcl11b sets pro-T cell fate by site-specific cofactor recruitment and by repressing Id2 and Zbtb16. *Nat. Immunol.*, **19**, 1427–1440.
55. Isoda,T., Moore,A.J., He,Z., Chandra,V., Aida,M., Denholtz,M., Piet van Hamburg,J., Fisch,K.M., Chang,A.N., Fahl,S.P., *et al.* (2017) Non-coding transcription instructs chromatin folding and

compartmentalization to dictate enhancer-promoter communication and T cell fate. *Cell*, **171**, 103–119.
56. Lessel,D., Gehbauer,C., Bramswig,N.C., Schluth-Bolard,C., Venkataramanappa,S., van Gassen,K.L.I., Hempel,M., Haack,T.B., Baresic,A., Genetti,C.A., *et al.* (2018) BCL11B mutations in patients affected by a neurodevelopmental disorder with reduced type 2 innate lymphoid cells. *Brain*, **141**, 2299–2311.
57. Qiao,F., Wang,C., Luo,C., Wang,Y., Shao,B., Tan,J., Hu,P. and Xu,Z. (2019) A De Novo heterozygous frameshift mutation identified in BCL11B causes neurodevelopmental disorder by whole exome sequencing. *Mol. Genet. Genomic Med.*, **7**, e897.
58. Prasad,M., Balci,T.B., Prasad,C., Andrews,J.D., Lee,R., Jurkiewicz,M.T., Napier,M.P., Colaiacovo,S., Guillen Sacoto,M.J. and Karp,N. (2020) BCL11B-related disorder in two canadian children: expanding the clinical phenotype. *Eur. J. Med. Genet.*, **63**, 104007.
59. Punwani,D., Zhang,Y., Yu,J., Cowan,M.J., Rana,S., Kwan,A., Adhikari,A.N., Lizama,C.O., Mendelsohn,B.A., Fahl,S.P., *et al.* (2016) Multisystem anomalies in severe combined immunodeficiency with mutant BCL11B. *N. Engl. J. Med.*, **375**, 2165–2176.
60. Grabarczyk,P., Winkler,P., Delin,M., Sappa,P.K., Bekeschus,S., Hildebrandt,P., Przybylski,G.K., Volker,U., Hammer,E. and Schmidt,C.A. (2018) The N-terminal CCHC zinc finger motif mediates homodimerization of transcription factor BCL11B. *Mol. Cell. Biol.*, **38**, e00368-17.
61. Lee,K.A.W., Bindereif,A. and Green,M.R. (1988) A small-scale procedure for preparation of nuclear extracts that support efficient transcription and pre-mRNA splicing. *Gene. Anal. Techn.*, **5**, 22–31.
62. Svilar,D., Vens,C. and Sobol,R.W. (2012) Quantitative, real-time analysis of base excision repair activity in cell lysates utilizing lesion-specific molecular beacons. *J. Visual. Exp.*, **66**, e4168.
63. Gaudreau-Lapierre,A., Garneau,D., Djerir,B., Coulombe,F., Morin,T. and Marechal,A. (2018) Investigation of protein recruitment to DNA lesions using 405 nm laser micro-irradiation. *J. Visual. Exp.*, **133**, e57410.
64. Schindelin,J., Arganda-Carreras,I., Frise,E., Kaynig,V., Longair,M., Pietzsch,T., Preibisch,S., Rueden,C., Saalfeld,S., Schmid,B., *et al.* (2012) Fiji: an open-source platform for biological-image analysis. *Nat. Methods*, **9**, 676–682.
65. Dorjsuren,D., Wilson,D.M., Beard,W.A., McDonald,J.P., Austin,C.P., Woodgate,R., Wilson,S.H. and Simeonov,A. (2009) A real-time fluorescence method for enzymatic characterization of specialized human DNA polymerases. *Nucleic Acids Res.*, **37**, e128.
66. Srivastava,D.K., Berg,B.J., Prasad,R., Molina,J.T., Beard,W.A., Tomkinson,A.E. and Wilson,S.H. (1998) Mammalian abasic site base excision repair. Identification of the reaction sequence and rate-determining steps. *J. Biol. Chem.*, **273**, 21203–21209.
67. Vadnais,C., Davoudi,S., Afshin,M., Harada,R., Dudley,R., Clermont,P.L., Drobetsky,E. and Nepveu,A. (2012) CUX1 transcription factor is required for optimal ATM/ATR-mediated responses to DNA damage. *Nucleic Acids Res.*, **40**, 4483–4495.
68. Paz-Elizur,T., Elinger,D., Leitner-Dagan,Y., Blumenstein,S., Krupsky,M., Berrebi,A., Schechtman,E. and Livneh,Z. (2007) Development of an enzymatic DNA repair assay formolecular epidemiology studies: Distribution of OGGactivity in healthy individuals. *DNA Repair*, **6**, 45–60.
69. Furth,E.E., Thilly,W.G., Penman,B.W., Liber,H.L. and Rand,W.M. (1981) Quantitative assay for mutation in diploid human lymphoblasts using microtiter plates. *Anal. Biochem.*, **110**, 1–8.
70. Lang,G.I. (2018) Measuring mutation rates using the Luria-Delbruck fluctuation assay. *Methods Mol. Biol.*, **1672**, 21–31.
71. Yao,Z., Aboualizadeh,F., Kroll,J., Akula,I., Snider,J., Lyakisheva,A., Tang,P., Kotlyar,M., Jurisica,I., Boxem,M., *et al.* (2020) Split intein-mediated protein ligation for detecting protein-protein interactions and their inhibition. *Nat. Commun.*, **11**, 2440.
72. Collins,A.R. (2009) Investigating oxidative DNA damage and its repair using the comet assay. *Mutat. Res.*, **681**, 24–32.
73. Kong,X., Mohanty,S.K., Stephens,J., Heale,J.T., Gomez-Godinez,V., Shi,L.Z., Kim,J.S., Yokomori,K. and Berns,M.W. (2009) Comparative analysis of different laser systems to study cellular responses to DNA damage in mammalian cells. *Nucleic Acids Res.*, **37**, e68.
74. Lan,L., Nakajima,S., Oohata,Y., Takao,M., Okano,S., Masutani,M., Wilson,S.H. and Yasui,A. (2004) In situ analysis of repair processes for oxidative DNA damage in mammalian cells. *Proc. Natl. Acad. Sci. U.S.A.*, **101**, 13738–13743.
75. Trivedi,R.N., Wang,X.H., Jelezcova,E., Goellner,E.M., Tang,J.B. and Sobol,R.W. (2008) Human methyl purine DNA glycosylase and DNA polymerase beta expression collectively predict sensitivity to temozolomide. *Mol. Pharmacol.*, **74**, 505–516.
76. Prasad,R., Beard,W.A., Strauss,P.R. and Wilson,S.H. (1998) Human DNA polymerase beta deoxyribose phosphate lyase. Substrate specificity and catalytic mechanism. *J. Biol. Chem.*, **273**, 15263–15270.
77. Grabarczyk,P., Delin,M., Roginska,D., Schulig,L., Forkel,H., Depke,M., Link,A., Machalinski,B. and Schmidt,C.A. (2021) Nuclear import of BCL11B is mediated by a classical nuclear localization signal and not the Kruppel-like zinc fingers. *J. Cell Sci.*, **134**, jcs258655.
78. Yin,B., Delwel,R., Valk,P.J., Wallace,M.R., Loh,M.L., Shannon,K.M. and Largaespada,D.A. (2009) A retroviral mutagenesis screen reveals strong cooperation between Bcl11a overexpression and loss of the Nf1 tumor suppressor gene. *Blood*, **113**, 1075–1085.
79. Serrano,M., Lin,A.W., McCurrach,M.E., Beach,D. and Lowe,S.W. (1997) Oncogenic ras provokes premature cell senescence associated with accumulation of p53 and p16INK4a. *Cell*, **88**, 593–602.
80. Weyemi,U., Lagente-Chevallier,O., Boufraqech,M., Prenois,F., Courtin,F., Caillou,B., Talbot,M., Dardalhon,M., Al Ghuzlan,A., Bidart,J.M., *et al.* (2012) ROS-generating NADPH oxidase NOX4 is a critical mediator in oncogenic H-ras-induced DNA damage and subsequent senescence. *Oncogene*, **31**, 1117–1129.
81. Mitsushita,J., Lambeth,J.D. and Kamata,T. (2004) The superoxide-generating oxidase Nox1 is functionally required for ras oncogene transformation. *Cancer Res.*, **64**, 3580–3585.
82. O'Neill,J.P., Brimer,P.A., Machanoff,R., Hirsch,G.P. and Hsie,A.W. (1977) A quantitative assay of mutation induction at the hypoxanthine-guanine phosphoribosyl transferase locus in Chinese hamster ovary cells (CHO/HGPRT system): development and definition of the system. *Mutat. Res.*, **45**, 91–101.
83. Luria,S.E. and Delbruck,M. (1943) Mutations of bacteria from virus sensitivity to virus resistance. *Genetics*, **28**, 491–511.
84. Svilar,D., Goellner,E.M., Almeida,K.H. and Sobol,R.W. (2011) Base excision repair and lesion-dependent subpathways for repair of oxidative DNA damage. *Antioxid. Redox Signal.*, **14**, 2491–2507.
85. Trivedi,R.N., Almeida,K.H., Fornsaglio,J.L., Schamus,S. and Sobol,R.W. (2005) The role of base excision repair in the sensitivity and resistance to temozolomide-mediated cell death. *Cancer Res.*, **65**, 6394–6400.
86. Dankort,D., Filenova,E., Collado,M., Serrano,M., Jones,K. and McMahon,M. (2007) A new mouse model to explore the initiation, progression, and therapy of BRAFV600E-induced lung tumors. *Genes Dev.*, **21**, 379–384.
87. Lee,A.C., Fenster,B.E., Ito,H., Takeda,K., Bae,N.S., Hirai,T., Yu,Z.X., Ferrans,V.J., Howard,B.H. and Finkel,T. (1999) Ras proteins induce senescence by altering the intracellular levels of reactive oxygen species. *J. Biol. Chem.*, **274**, 7936–7940.
88. Collado,M., Gil,J., Efeyan,A., Guerra,C., Schuhmacher,A.J., Barradas,M., Benguria,A., Zaballos,A., Flores,J.M., Barbacid,M.,

et al. (2005) Tumour biology: senescence in premalignant tumours. *Nature*, **436**, 642.
89. Bartkova,J., Rezaei,N., Liontos,M., Karakaidos,P., Kletsas,D., Issaeva,N., Vassiliou,L.V., Kolettas,E., Niforou,K., Zoumpourlis,V.C., *et al.* (2006) Oncogene-induced senescence is part of the tumorigenesis barrier imposed by DNA damage checkpoints. *Nature*, **444**, 633–637.
90. Fujita,K., Mondal,A.M., Horikawa,I., Nguyen,G.H., Kumamoto,K., Sohn,J.J., Bowman,E.D., Mathe,E.A., Schetter,A.J., Pine,S.R., *et al.* (2009) p53 isoforms Delta133p53 and p53beta are endogenous regulators of replicative cellular senescence. *Nat. Cell Biol.*, **11**, 1135–1142.
91. Kuilman,T., Michaloglou,C., Vredeveld,L.C., Douma,S., van Doorn,R., Desmet,C.J., Aarden,L.A., Mooi,W.J. and Peeper,D.S. (2008) Oncogene-induced senescence relayed by an interleukin-dependent inflammatory network. *Cell*, **133**, 1019–1031.
92. Michaloglou,C., Vredeveld,L.C., Soengas,M.S., Denoyelle,C., Kuilman,T., van der Horst,C.M., Majoor,D.M., Shay,J.W., Mooi,W.J. and Peeper,D.S. (2005) BRAFE600-associated senescence-like cell cycle arrest of human naevi. *Nature*, **436**, 720–724.
93. Courtois-Cox,S., Genther Williams,S.M., Reczek,E.E., Johnson,B.W., McGillicuddy,L.T., Johannessen,C.M., Hollstein,P.E., MacCollin,M. and Cichowski,K. (2006) A negative feedback signaling network underlies oncogene-induced senescence. *Cancer Cell*, **10**, 459–472.
94. Campisi,J. (2013) Aging, cellular senescence, and cancer. *Annu. Rev. Physiol.*, **75**, 685–705.
95. Young,T.W., Mei,F.C., Yang,G., Thompson-Lanza,J.A., Liu,J. and Cheng,X. (2004) Activation of antioxidant pathways in ras-mediated oncogenic transformation of human surface ovarian epithelial cells revealed by functional proteomics and mass spectrometry. *Cancer Res.*, **64**, 4577–4584.
96. Trachootham,D., Zhou,Y., Zhang,H., Demizu,Y., Chen,Z., Pelicano,H., Chiao,P.J., Achanta,G., Arlinghaus,R.B., Liu,J., *et al.* (2006) Selective killing of oncogenically transformed cells through a ROS-mediated mechanism by beta-phenylethyl isothiocyanate. *Cancer Cell*, **10**, 241–252.
97. Trachootham,D., Alexandre,J. and Huang,P. (2009) Targeting cancer cells by ROS-mediated mechanisms: a radical therapeutic approach?*Nat. Rev. Drug Discov.*, **8**, 579–591.
98. Singh,A., Misra,V., Thimmulappa,R.K., Lee,H., Ames,S., Hoque,M.O., Herman,J.G., Baylin,S.B., Sidransky,D., Gabrielson,E., *et al.* (2006) Dysfunctional KEAP1-NRF2 interaction in non-small-cell lung cancer. *PLoS Med.*, **3**, e420.
99. Luo,J., Emanuele,M.J., Li,D., Creighton,C.J., Schlabach,M.R., Westbrook,T.F., Wong,K.K. and Elledge,S.J. (2009) A genome-wide RNAi screen identifies multiple synthetic lethal interactions with the Ras oncogene. *Cell*, **137**, 835–848.
100. Ramdzan,Z.M., Ginjala,V., Pinder,J.B., Chung,D., Donovan,C.M., Kaur,S., Leduy,L., Dellaire,G., Ganesan,S. and Nepveu,A. (2017) The DNA repair function of CUX1 contributes to radioresistance. *Oncotarget*, **8**, 19021–19038.
101. Ramdzan,Z.M., Vickridge,E., Faraco,C.C.F. and Nepveu,A. (2021) CUT domain proteins in DNA repair and cancer. *Cancers (Basel)*, **13**, 2953.
102. Vickridge,E., Faraco,C.C.F. and Nepveu,A. (2022) Base excision repair accessory factors in senescence avoidance and resistance to treatments. *Cancer Drug Resist*, **5**, 703–720.
103. Starcevic,D., Dalal,S. and Sweasy,J.B. (2004) Is there a link between DNA polymerase beta and cancer?*Cell Cycle*, **3**, 998–1001.
104. Lang,T., Maitra,M., Starcevic,D., Li,S.X. and Sweasy,J.B. (2004) A DNA polymerase beta mutant from colon cancer cells induces mutations. *Proc. Natl. Acad. Sci. U.S.A.*, **101**, 6074–6079.
105. Ramdzan,Z.M. and Nepveu,A. (2014) CUX1, a haploinsufficient tumour suppressor gene overexpressed in advanced cancers. *Nature Rev. Cancer*, **14**, 673–682.
106. Visschers,I.G.S., Van Dam,N.M. and Peters,J.L. (2018) Quantification of thrips damage using Ilastik and ImageJ Fiji. *Bio Protoc*, **8**, e2806.

Received: June 14, 2023. **Revised:** October 13, 2023. **Editorial Decision:** October 17, 2023. **Accepted:** October 23, 2023